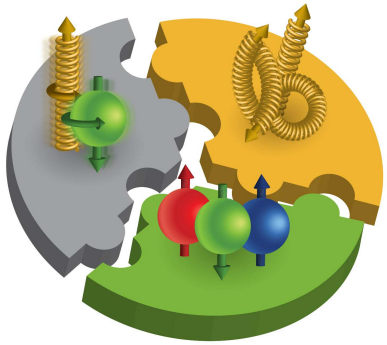

Hadron Polarimetry at the Electron-Ion Collider

Challenges and Solutions

Frank Rathmann, Vera Shmakova
for the EIC Polarimetry Group

Brookhaven National Laboratory

DNP 2025, October 17–20, 2025
Fall Meeting of the APS Division of Nuclear Physics, Chicago, IL
https://indico.phy.anl.gov/event/58/overview

Contents I

Introduction

Hadron polarimetry requirements for the EIC I

Deliverables

- The EIC will use polarized **protons** ($\vec{p}$) and **helions** ($\vec{h} = {}^{3}\overrightarrow{\mathrm{He}}$), later on deuterons ($\vec{d}$), and heavier nuclei like lithium ${}^{6,7}\overrightarrow{\mathrm{Li}}$) may be needed.
- **The EIC promises to provide proton beam polarizations of $P \geq 0.7$ with a relative uncertainty of $\Delta P/P \leq 1\%$.**
- Polarization calibration needed for each ion species as presently done:
  - elastic scattering of identical particles $\Rightarrow$ beam polarization inferred from known target polarization.
- **Absolute proton beam polarization calibration relies on measured nuclear polarization of atomic jet using Breit-Rabi polarimeter.**

Hadron polarimetry requirements for the EIC II

Instruments

- Hadron polarimeter (absolute) in **IP4**
- pC polarimeter (relative) in **IP4** and **IP6** (between spin rotators)

Polarimeters shall determine:

- Bunch polarization profile in x, y, z
- Polarization lifetime
  - For EIC physics, projection of $\vec{P}$ on stable spin axis required, no in-plane polarization.
- Polarization vector $\vec{P}$ per bunch

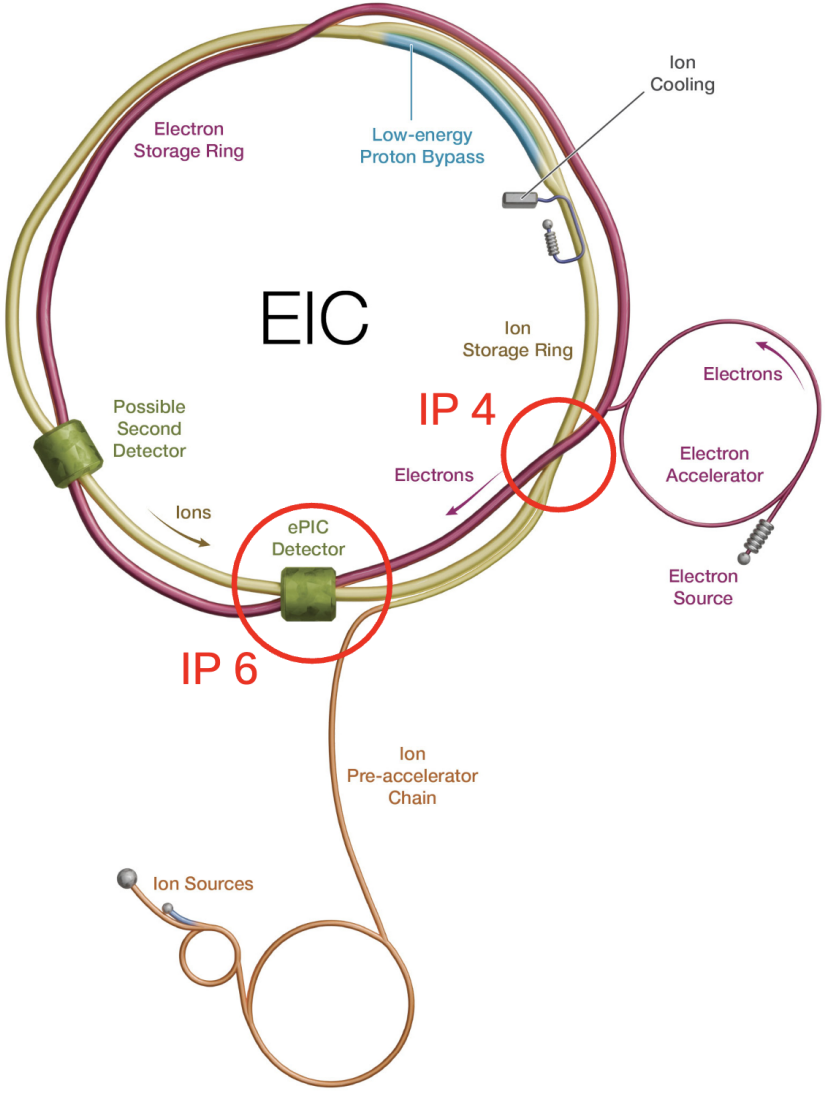

Asymmetry and polarization

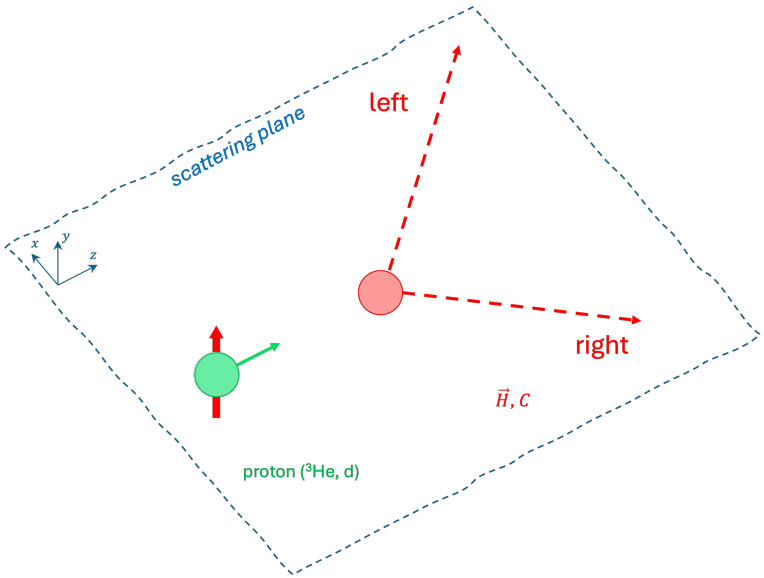

- Spin-dependent cross section

$$\sigma = \sigma_0(1 + A_y P_y \cos\phi) \quad (1)$$

  - Unpolarized cross section σ_0
  - P_y vertical component of beam polarization $\vec{P} = (P_x, P_y, P_z)$
  - Analyzing power $A_y = \frac{1}{P_y}\frac{\sigma^{\text{left}} - \sigma^{\text{right}}}{\sigma^{\text{left}} + \sigma^{\text{right}}}$
  - Azimuth of scattered particle ϕ

Coulomb-nuclear interference (CNI) (see slide 43).)

- A_y: measure of polarization sensitivity of scattering process
- **At AGS and RHIC energies, no scattering processes available with A_y known to sufficient accuracy for $\Delta P/P \leq 0.01$** (see [1].
- **Interference of EM and strong interaction at small scattering angles provides sizable analyzing power for elastic pp (and pN) scattering.**

Instruments

Instruments for absolute and relative polarimetry

Two devices

- **HJET polarimeter**

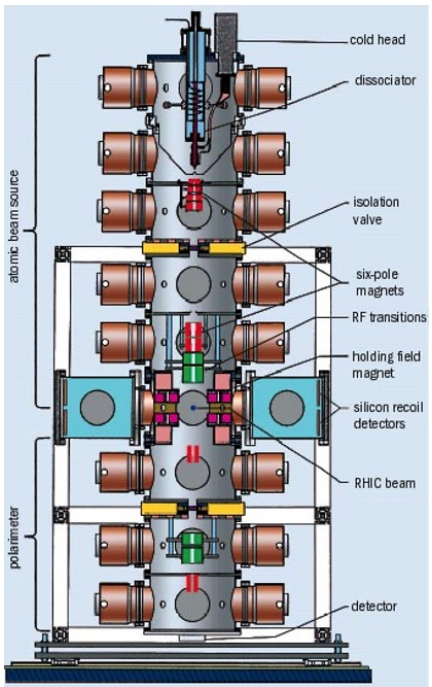

  - **absolute, slow**

$$\frac{\Delta P}{P} \approx 3\% \text{ per } 4 \text{ hour} \quad (2)$$

- **pC polarimeters**

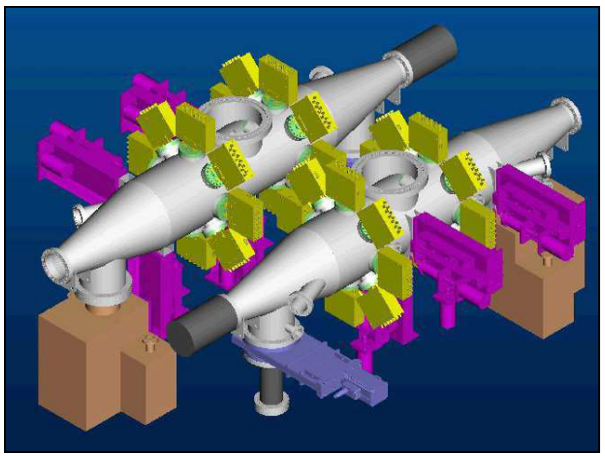

  - **fast, relative**
  - transverse profiles of polarization

$$\frac{\Delta P}{P} < 1\% \text{ per scan} \quad (3)$$

Present RHIC detector system at the polarized jet target

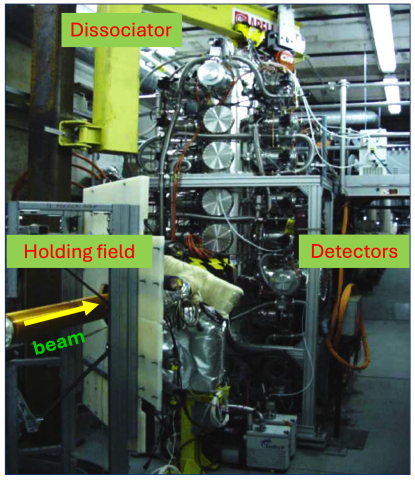

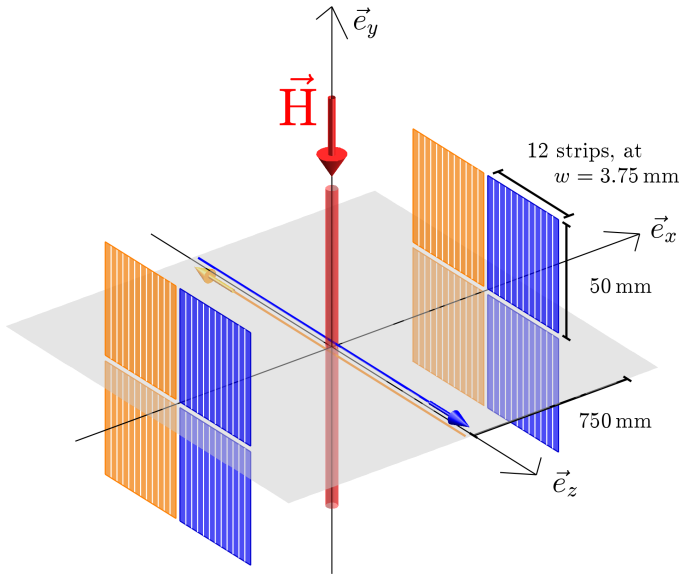

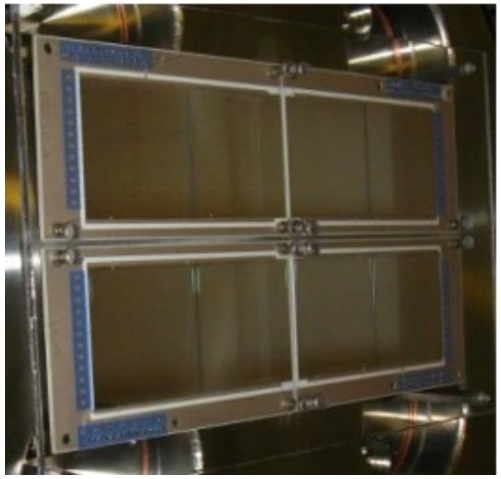

Eight Si strip detectors

- 12 vertical strips, 3.75 mm pitch, 500 µm thickness

With present setup of L-R detectors and guide field B_y

- Only vertical component P_y measurable via L-R asymmetry near $\theta = 90°$.

Present CNI polarimeter setup

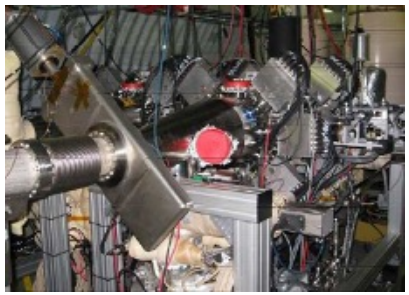

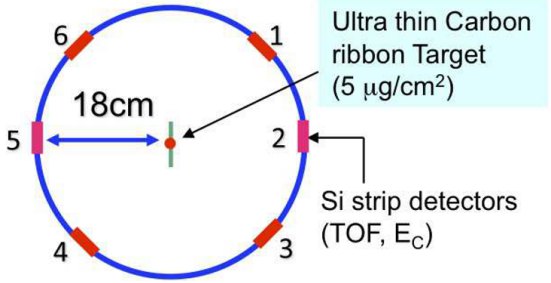

CNI setup with 6 Si detectors at different azimuth at each target enables

- determination of polarization components P_x and P_y
- determination of polarization profile along x and y
- Due to parity violation, $A_z \approx 0$ (no longitudinal analyzing power) $\rightarrow$ P_z not measurable with *unpolarized* target

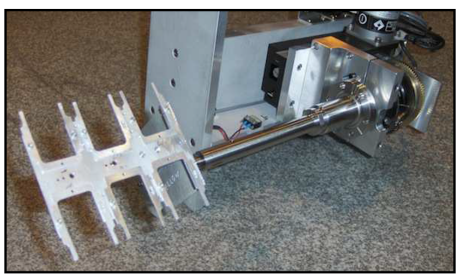

Ultra-thin ribbon targets

- 8 target holder inside beam pipe
- 2 holders per beam for x and y
- 6 targets per holders, 48 in total
- Targets $\approx 10\,\mu\text{m} \times 50\,\text{nm}$, hand crafted by D. Steski & team

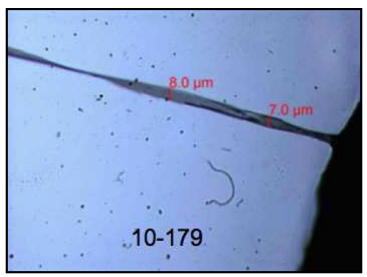

Absolute beam polarization

Absolute polarization from polarized hydrogen jet I

Breit-Rabi polarimeter

- Capable to determine absolute polarization Q of atomic beam, i.e., electron and proton polarization of hydrogen atoms, with accuracy $\Delta Q/Q \lesssim 1\%$.
  - No solid estimates available that fully encapsulate the BRP measurement systematics at the HJET on the $\approx 1\%$ level (see F. Rathmann et al., "Eliminating beam-induced depolarizing effects in the hydrogen jet target for high-precision proton beam polarimetry at the Electron-Ion Collider," (2025), 2508.01366.).

Beam polarization calibration

1. Proton beam passes through target of polarized H atoms of known polarization Q

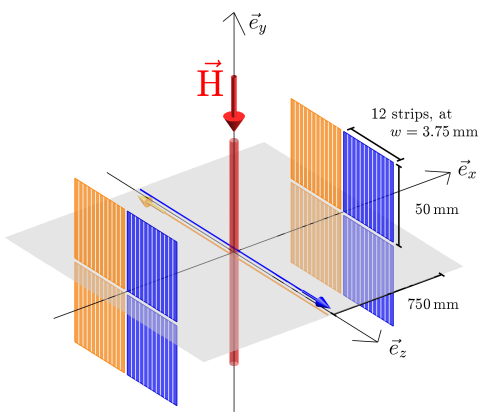

Absolute polarization from polarized hydrogen jet II

Beam polarization calibration

2. Measure number of scattered particles in left (L) and right (R) detectors (at $\phi = 0$ and $\phi = \pi$, respectively).
3. Sign of Q is periodically reversed to compensate for asymmetries caused by differences in detector geometry or efficiency in L and R directions.
4. This determines target asymmetry

$$\epsilon_{\text{target}} = \frac{\text{L} - \text{R}}{\text{L} + \text{R}} = A_y \cdot Q\,. \tag{4}$$

5. Measurement of corresponding asymmetry with beam particles determines ϵ_{beam}. In elastic pp scattering, and more general in the elastic scattering of *identical* particles, A_y same regardless of which proton is polarized.
6. Absolute beam polarization given by

$$\boxed{P = \frac{\epsilon_{\text{beam}}}{\epsilon_{\text{target}}} \cdot Q} \tag{5}$$

Beam-induced target depolarization

Beam-induced target depolarization at RHIC and EIC

- At EIC, the bunch repetition frequency is much larger than at RHIC → **investigate beam-induced depolarization of target atoms** (see F. Rathmann et al., "Eliminating beam-induced depolarizing effects in the hydrogen jet target for high-precision proton beam polarimetry at the Electron-Ion Collider," (2025), 2508.01366.).

RHIC situation:

- Time period between two adjacent bunches: $\tau_\mathrm{b} = \frac{\tau_\mathrm{rev}}{N_b} = 106.598\,\mathrm{ns}$
- Number of stored bunches $N_b = 120$
- Bunch frequency $f_\mathrm{b} = \frac{1}{\tau_\mathrm{b}} = 9.381\,\mathrm{MHz}$
- Large number of harmonics contribute to induced magnetic high-frequency field close to RHIC beam, as bunches are short ($\sigma_t \approx 1.8\,\mathrm{ns}$)

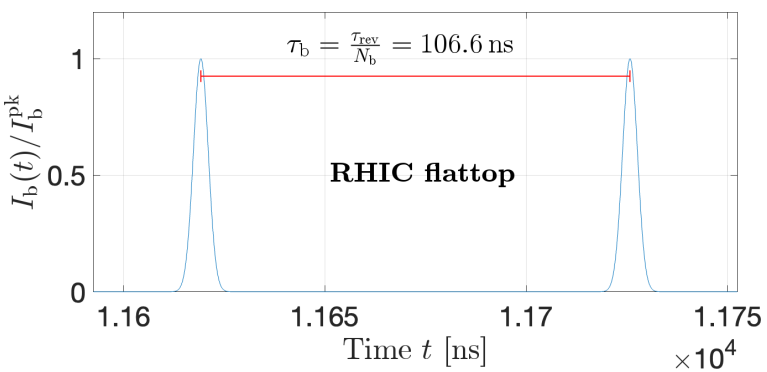

Hyperfine states of hydrogen

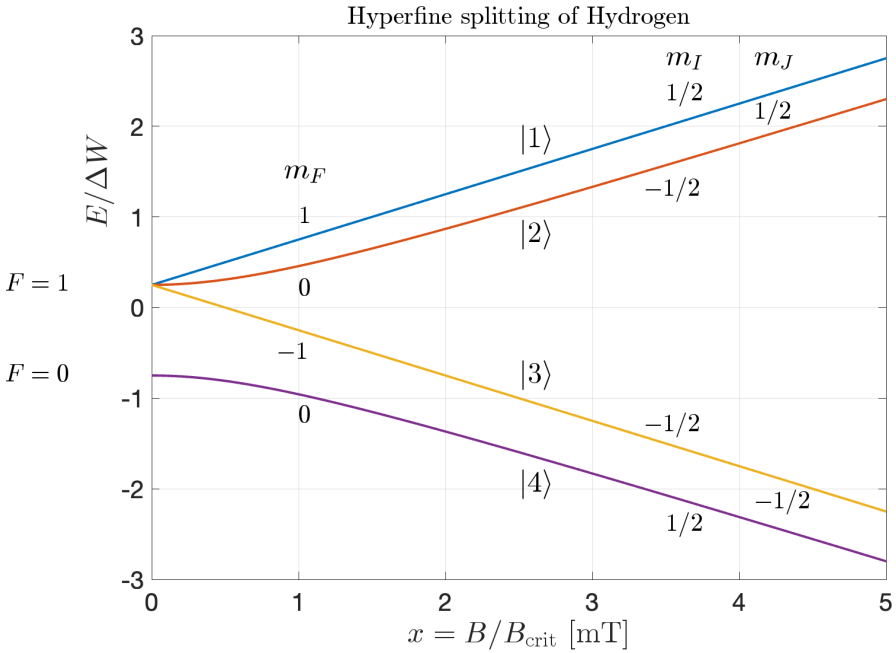

Critical field B_c (see slide 45)

- Zeeman energy $g_J \mu_B B$ comparable to E_{hfs}
- $E_{\text{hfs}} \approx 5.874 \times 10^{-6}$ eV ($\approx$1420 MHz [3]):
- $B_c = 50.7$ mT

Transition frequencies

- Transition frequency between two hyperfine states $|i\rangle$ and $|j\rangle$ given by:

$$f_{ij} = \frac{E_{|i\rangle}(B) - E_{|j\rangle}(B)}{h} \tag{6}$$

- **When f_{ij} matches one of the beam harmonics at a certain holding field $|\vec{B}|$, resonant depolarization occurs** [4]

Single bunch and convolution

- (Gaussian) bunch in RHIC

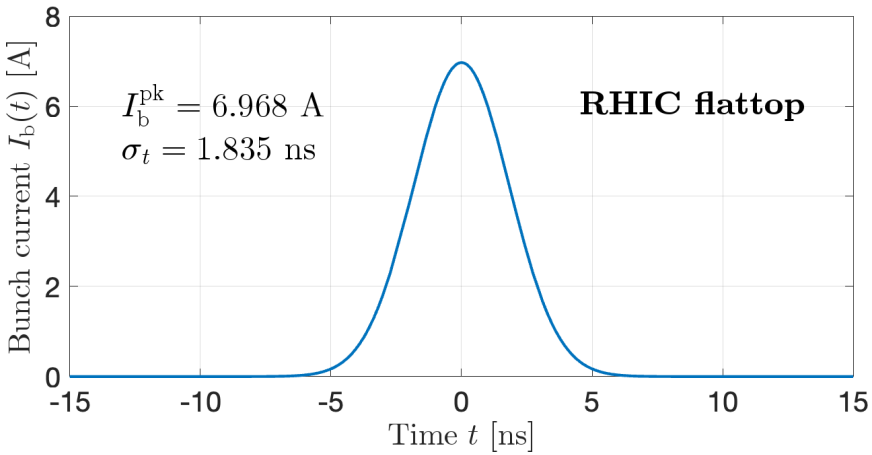

Pulse shape described by

$$f(t) = \frac{Q}{\sqrt{2\pi}\sigma_t} \exp\left(-\frac{t^2}{2\sigma_t^2}\right) \quad (7)$$

- Gaussian convoluted with (finite) series of delta functions.

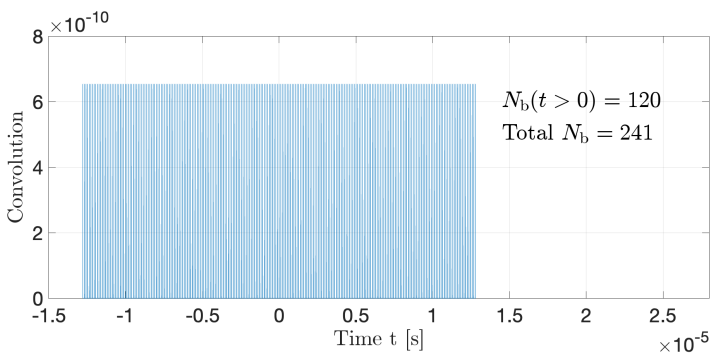

Total beam current as function of time t

$$I(t) = \int_{-\infty}^{\infty} f(t-\xi) \sum_{k=-\infty}^{\infty} \delta\left(\xi - k\frac{\tau_{rev}}{N_b}\right) d\xi \quad (8)$$

Produced radio-frequency fields from FFT of convolution

- Single-sided amplitude spectrum of FFT
- x-axis converted to frequency

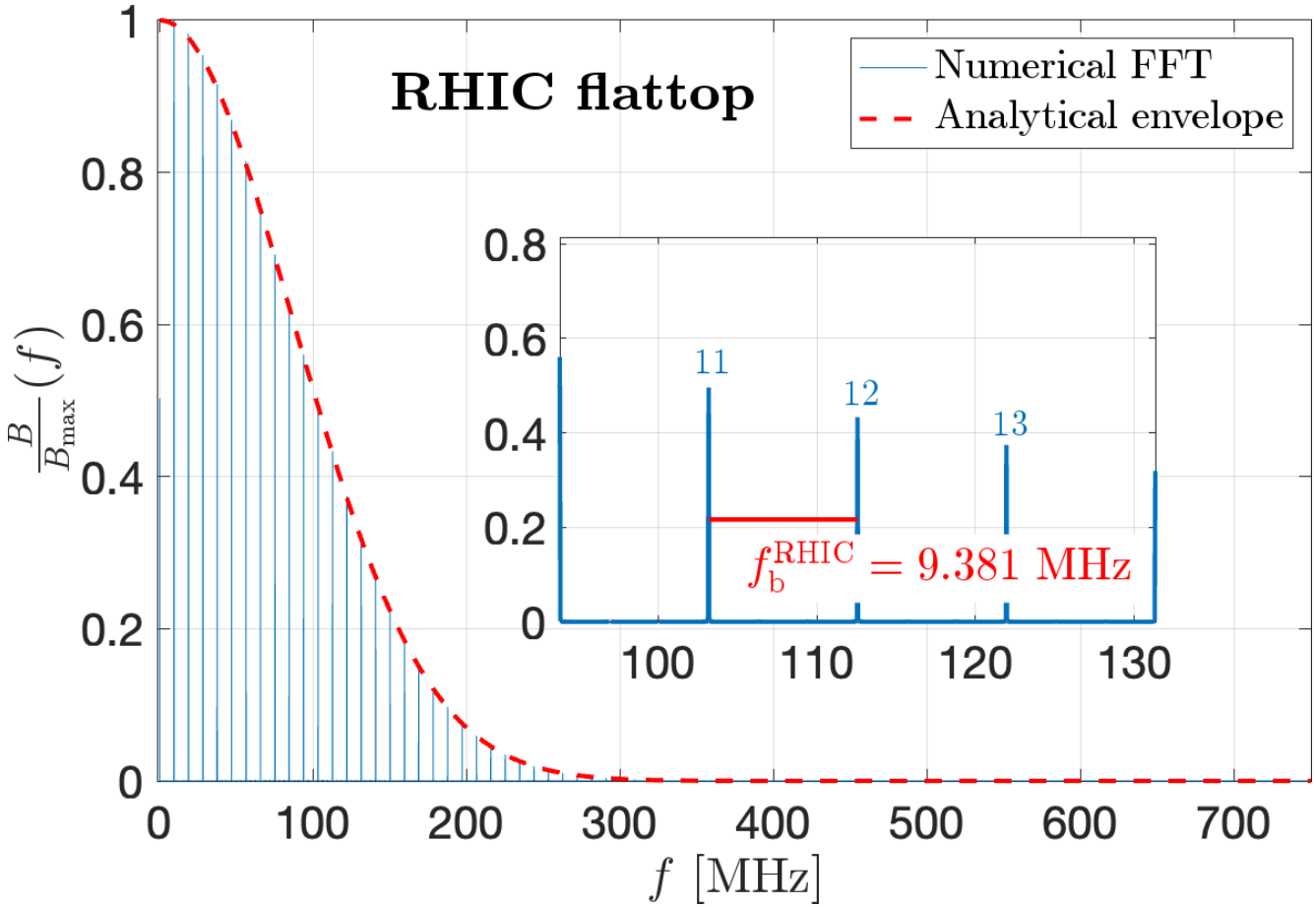

Transition frequencies between hyperfine states of H

Using Zeeman splitting (see slide 16, Eq. (6))

- $\vec{B}_0$ is the static guiding field; $\vec{B}_1(t)$ is the RF field.
- Magnetic–moment precession of $\vec{\mu}$ about $\vec{B}_{\text{tot}}$

$$\frac{\mathrm{d}\vec{s}}{\mathrm{d}t} = \vec{\mu} \times \vec{B}_{\text{tot}} \tag{9}$$

- Adiabatic fast passage commonly used in ABS operation.
- Determine transition frequencies f_{ij} between states $|i\rangle$ and $|j\rangle$.
- **Selection rules** (quantization axis $\vec{e}_z \parallel \vec{B}_0$ [5, 6]):
  - π **transitions** ($\vec{B}_1 \perp \vec{B}_0$):
    - Weak field ($B_0 \ll B_{\text{crit}}$): $\Delta F = 0, \quad \Delta m_F = \pm 1$
    - Strong field ($B_0 \gg B_{\text{crit}}$): $\Delta m_J = \pm 1, \quad \Delta m_I = 0$
  - σ **transitions** ($\vec{B}_1 \parallel \vec{B}_0$):
    - Weak field: $\Delta F = \pm 1, \quad \Delta m_F = 0, \pm 1 \quad (F{=}0 \nleftrightarrow F{=}0)$
    - Strong field: $\Delta m_J = 0, \quad \Delta m_I = 0, \pm 1$

Transition frequencies between hyperfine states of H

Possible transitions

- Single photon transitions in H: f_{12}^{π}, f_{23}^{π}, f_{14}^{σ}, f_{24}^{σ}, and f_{34}^{σ}.
- Transition $f_{13}^{2\gamma}$ with $\Delta m_F = 2$ requires two photons.

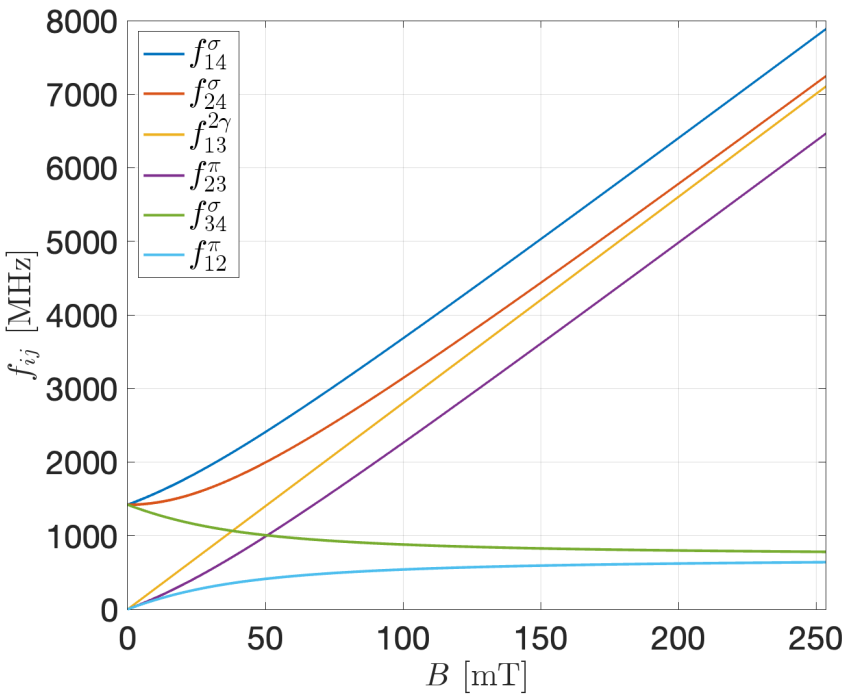

- For $n = 4$ hyperfine states, $\binom{n}{2} = 6$ transitions possible.
- f_{14}^{σ} and f_{23}^{π} transitions leave m_I unchanged $\Rightarrow$ don't affect nuclear polarization.

Hyperfine transitions in H from bunch fields at RHIC

Depolarization occurs when f_{ij} multiple of bunch frequency f_b^{RHIC}

- HJET injects states $|1\rangle + |4\rangle$ ($p^{\uparrow}$) and $|2\rangle + |3\rangle$ ($p^{\downarrow}$).
  - What is exact magnitude and orientation of $\vec{B}^{\mathrm{HJET}}$? **Visit issue after run 25**

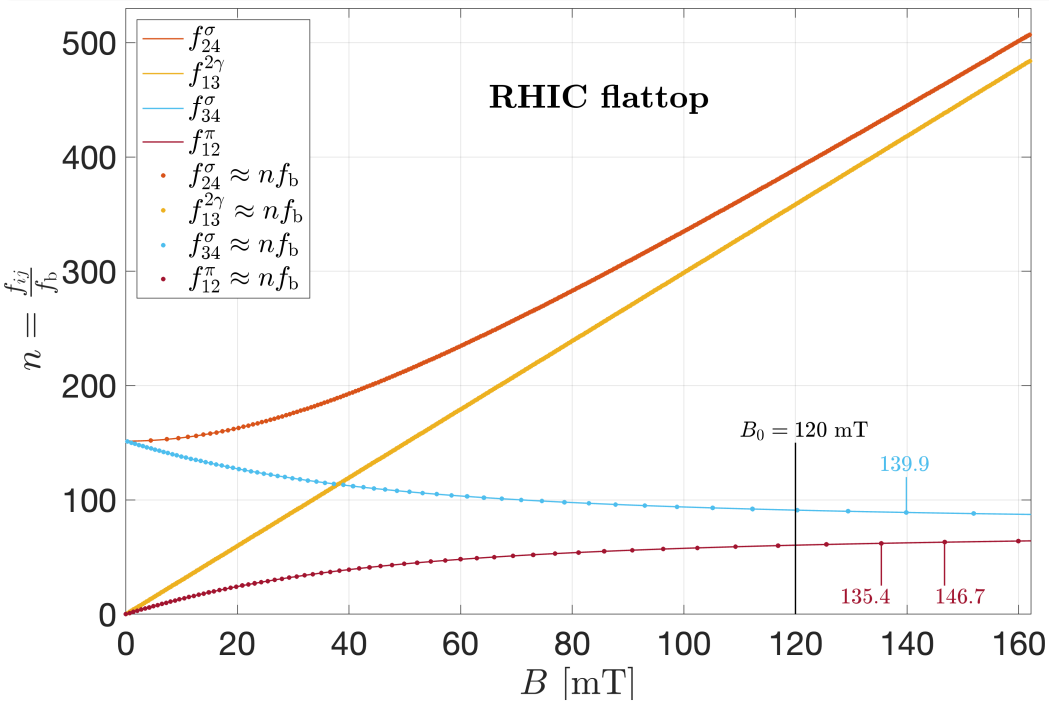

- $f_{ij}(B) \approx n\, f_b^{\mathrm{RHIC}}$, $n \in \mathbb{N}$
- No depolarization from same $m_I \Rightarrow f_{14}^{\sigma}$, f_{23}^{π} omitted

HJET at RHIC operated in safe region around $B_y = 120\,\mathrm{mT}$

- At RHIC, transitions with $\frac{f_{ij}}{f_b^{\mathrm{RHIC}}} \gtrsim 350$ were ignored
- Don't know exactly at which harmonic number, depolarization sets in.

Beam bunch parameters for RHIC and EIC

RHIC and EIC flattop

Metric	**RHIC**	**EIC flattop**
Total beam energy E_{beam} [GeV]	255	275
Protons per bunch N_p [10^{10}]	20	6.9
Number of bunches N_b	120	1160
Bunch length σ_L [m]	0.55	0.06
Temporal bunch width σ_t [ns]	1.835	0.200
Bunch spacing τ_b [ns]	106.598	11.027
Bunch frequency f_b [MHz]	9.381	90.683

Bunch-induced radio-frequency fields at EIC flattop

- Bunch in EIC, $\sigma_t = 0.2\,\text{ns}$
- $\tau_\text{b} = 11.027\,\text{ns}$
- $N_b = 1160$ stored bunches
- $f_\text{b} = 90.683\,\text{MHz}$

- Single-sided amplitude spectrum of FFT

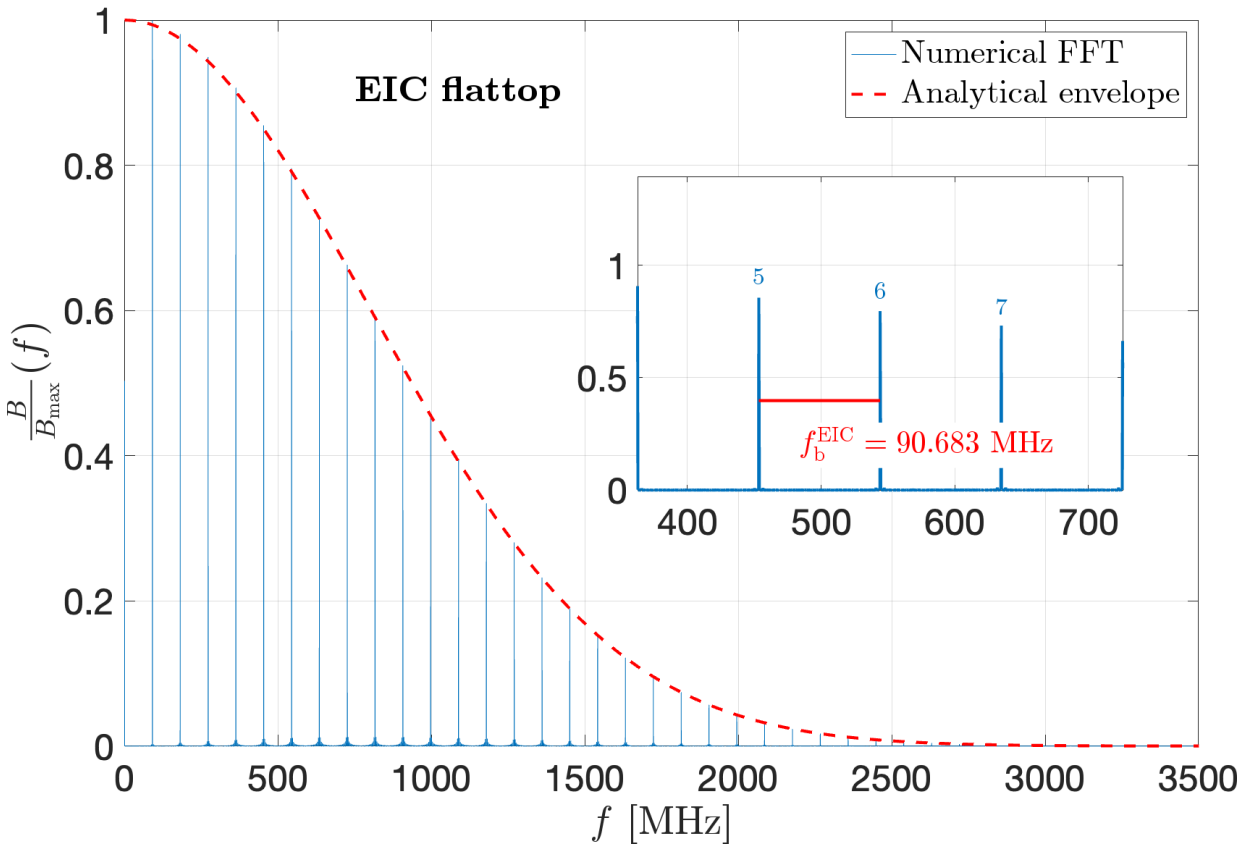

Hyperfine transitions in H from bunch fields at EIC

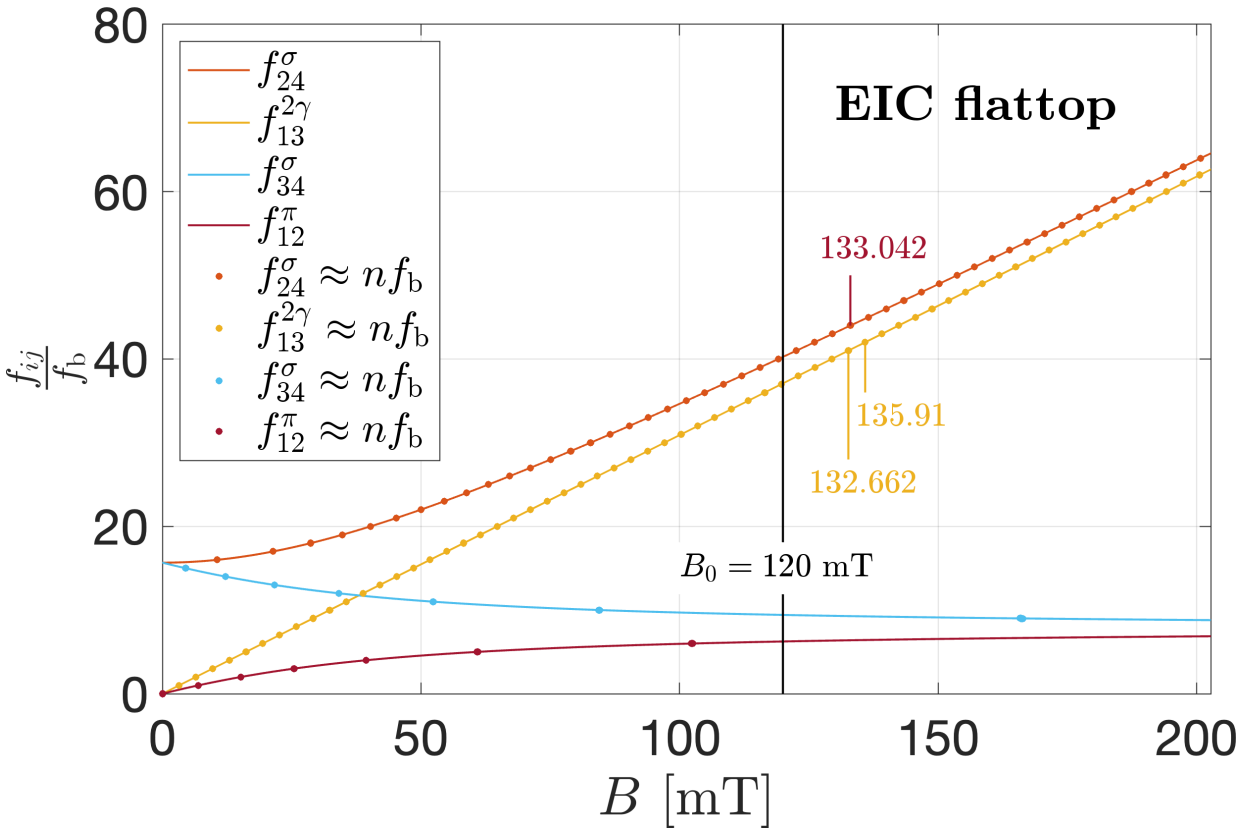

As before, depolarization occurs (numerically) when $f_{ij}(B) \approx n\, f_{\mathrm{b}}^{\mathrm{EIC}}$, $n \in \mathbb{N}$.

In contrast to RHIC, for $B < 120\,\mathrm{mT}$

- **All transitions below harmonic number ≈ 35 would contribute at EIC!**

Elimination of beam-induced H target depolarization at EIC

Solutions

1. At RHIC, B-field was moved to $\approx 120\,\mathrm{mT}$ and $\frac{f_{ij}}{f_{\mathrm{b}}^{\mathrm{RHIC}}} \geq 350$ ignored (slide 21)
2. **For EIC: $\Rightarrow$ push harmonics to ≥ 100 $\Rightarrow$ holding field $\geq 400\,\mathrm{mT}$**

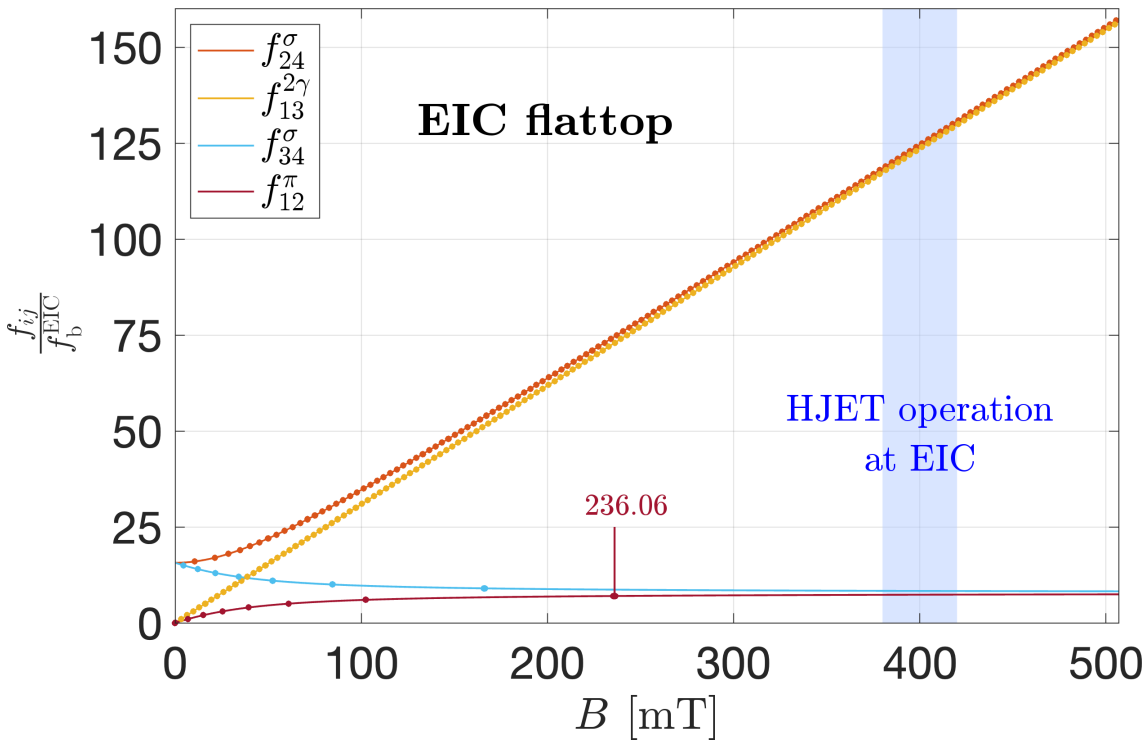

Resonances f_{34}^{σ} and f_{12}^{π}

- Become harmless (die out) above $\approx 236.06\,\mathrm{mT}$

pC polarimetry

Will carbon fiber targets survive at EIC?

Estimated target heating using code by Peter Thieberger (BNL)

- Increased beam sizes at EIC $\Rightarrow$ thin fibers remain applicable for EIC.
- RF heating of holders more severe at EIC due to shorter bunches.
  $\Rightarrow$ **optimize RF design of target holders**

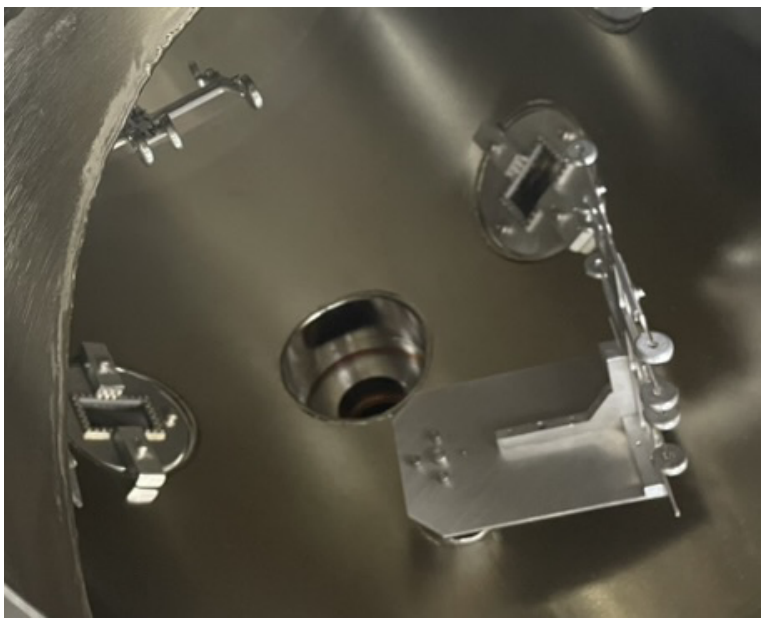

- Direct temperature measurements of targets is in progress (see slide 61)

Carbon target temperatures from Thieberger's model

Typical conditions, assuming round EIC beam

- **RHIC:** 250 GeV, 111 bunches, 16×10^{10} protons/bunch, $\sigma_r^{95} = 0.68$ mm.
- **EIC:** 275 GeV, 1160 bunches, 6.9×10^{10} protons/bunch, $\sigma_r^{95} = 1.2$ mm.

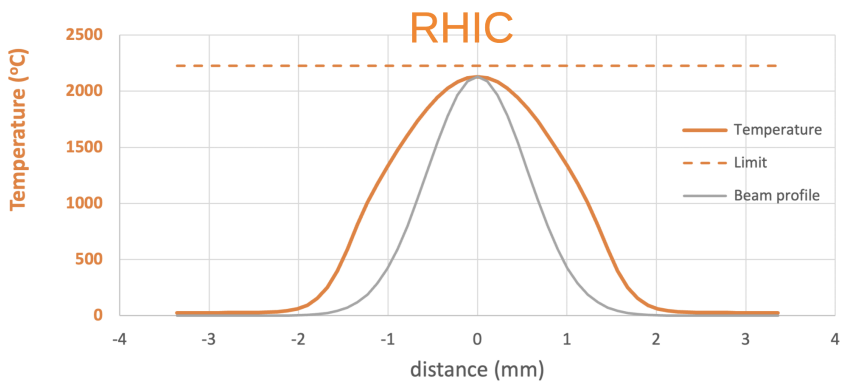

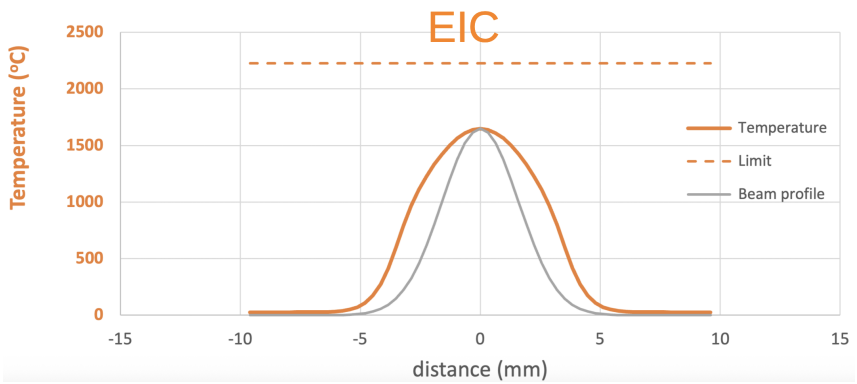

Thermal modeling of carbon ribbon targets

- Despite higher EIC beam energy and total current, the larger transverse beam size lowers power density and keeps the peak temperature below the carbon sublimation temperature $T_{\text{sub}} = 3915$ K [7].
- For pC ribbons in UHV, conservative continuous operation is typically below 3200 K to 3500 K to limit mass loss (see slide 62), but Thieberger's code [8] uses $T_{\text{melt}} = 2227$ K while carbon sublimes.

More complete picture using asymmetric beams at EIC

RHIC, EIC injection and EIC flattop

Metric	**RHIC**	T_{max} **[K]**	**EIC inj.**	T_{max} **[K]**	**EIC flattop**	T_{max} **[K]**
Target length ℓ [mm])	**25**		**50**		**50**	
Number of bunches	120		290		1160	
Protons / bunch ($\times 10^{10}$)	20.0		27.6		6.9	
σ_x^{95} [mm]	0.56	2130	8.60	**52**	3.94	**869**
σ_y^{95} [mm]	0.56	2130	1.69	**600**	0.66	**2665**
Equiv. round σ_r^{95} [mm]	0.56	2130	3.81	144	1.61	1610
$4\sigma_x^{95}$ [mm]	2.24		34.4		15.8	
$4\sigma_y^{95}$ [mm]	2.24		6.76		2.64	
Coverage $\ell/(4\sigma_x^{95})$	11.2		**1.45**		3.16	
Coverage $\ell/(4\sigma_y^{95})$	11.2		7.40		18.9	

Comments

1. Equivalent round size for thermal modeling: $\sigma_r^{95} = \sqrt{\sigma_x^{95}\,\sigma_y^{95}}$.
2. Rotation of setup by $\approx 45^\circ$ about $\vec{e}_z \Rightarrow T < T_{sub}$ at EIC injection for y' scan.
3. Length of horizontal ribbon is limiting case at EIC injection.

Wakefield simulations (pC target system)

Medani Sangroula (BNL)

- Wakefields from pC chamber and target holder near beam critical at EIC due to short bunches and rich harmonic content.
- Objective: minimize longitudinal impedance $Z_{\parallel}(f)$ and local power.
- Design lever: dielectric holder (e.g. Al_2O_3) with thin conductive coating for charge control; metallic features are RF-shielded.

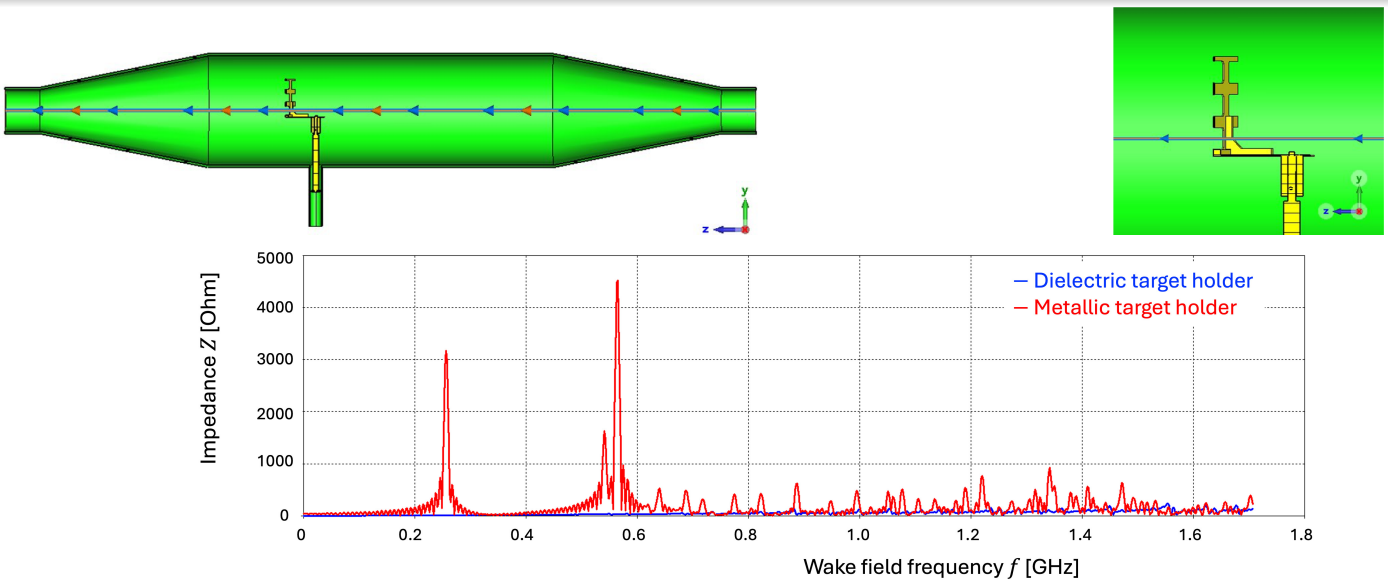

Wake impedance $Z(f)$: metallic (Al holder in SS chamber) vs. dielectric (Al_2O_3) holder

Findings

- Dielectric holders (e.g. Al_2O_3) reduce wake impedance vs. metallic designs.
- Thin conductive coating (charge) $\Rightarrow$ negligible impact on $Z(\omega)$.

Wakefield simulations (holder positioning)

- Move the dielectric target holder away from beam (0 mm → 38.1 mm → 76.2 mm).
- Goal: reduce wake potential $W(s)$ and local RF power deposition near the intercept.

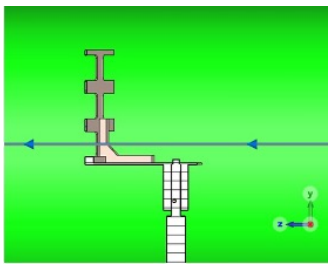

Target holder at 0 mm.

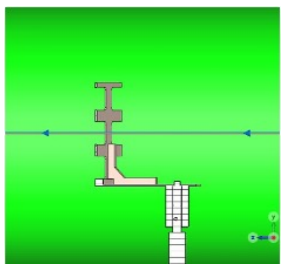

Target holder at 38.1 mm.

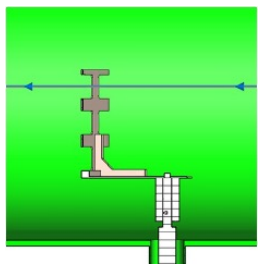

Target holder at 76.2 mm.

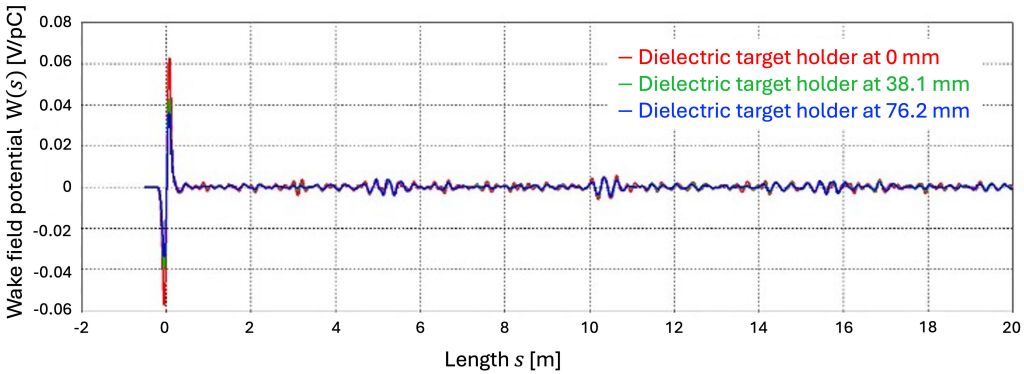

Wake potential $W(s)$: systematic reduction with increasing displacement toward chamber wall.

Findings

- Displacing dielectric holder away from beam reduces $W(s)$ across band of interest.
- Recommendation: RF shielding of nearby ports/feedthroughs.
- One-target-in-chamber minimizes impedance and simplifies operation.

Other polarized beam species

Polarized ^{3}He Atomic Beam Source

Original MIT development for nEDM exp't at Oakridge

- Prajwal T. MohanMurthy, J. Kelsey, J. Dodge, R. Redwine, R. Milner, P. Binns, B. O'Rourke
- nEDM experiment at ORNL discontinued

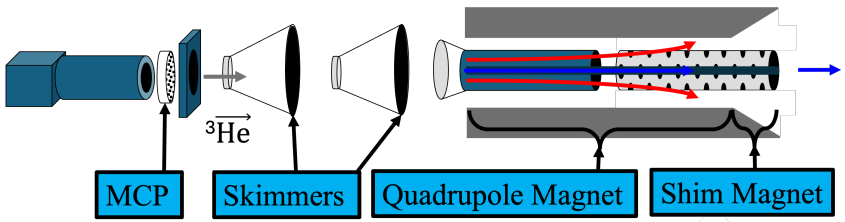

$^3\vec{\text{He}}$: quadrupole magnet selects spins
- **1.3 K ≈ 86 μeV**
- $\Delta E = \mu_m \approx 67$ neV/T
- initial angle very important

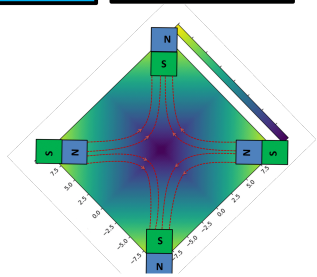

Atomic flux

- With $1 \times 10^{14}\,\text{s}^{-1} \Rightarrow$ bare-jet $d_t \approx 1.3 \times 10^{10}\,\text{cm}^{-2}$
  - Assumptions: $D = 1.0\,\text{cm}$ (uniform), $L = 1\,\text{cm}$, $T = 1.3\,\text{K}$.
- With storage cell (molecular flow, $T = 77\,\text{K}$): $d_t \approx 1.0 \times 10^{12}\,\text{cm}^{-2}$
  - Geometry: $\ell_{\text{inj}} = 10\,\text{cm}$, $\ell_{\text{up}} = \ell_{\text{down}} = 30\,\text{cm}$, $\ell_t = 60\,\text{cm}$ (see slide 70).
- **Well-suited for absolute $^3\vec{\text{He}}^{++}$ beam polarimetry at EIC.**

Absolute polarimetry of $\vec{d}$ beams

Polarized atomic deuterium jet

- Atomic beam sources efficiently produce beams of deuterium atoms
- Ideal would be the use of dual-function RF transition units for $\vec{\text{H}}$ and $\vec{\text{D}}$ atoms [9].
- With vector and tensor polarization accurately determined by BRP, absolute beam polarimetry based on $\vec{d}\vec{d}$ elastic scattering becomes possible
  - + B_x, B_y, B_z options will allow reconstruction of beam polarization $\vec{P} = (P_x, P_y, P_z)$ vector, incl. tensor components (see slide 47).

EIC hadron polarimetry at IP4

Carbon, polarized H, and ^{3}He gas targets at a single IP

- **Co–location** minimizes spin transport between devices
- **Common services:** unified slow controls and DAQ.
- **Functional roles:** carbon ribbon(s) for fast relative P scans; polarized H (HJET) and ^{3}He for absolute P calibration.

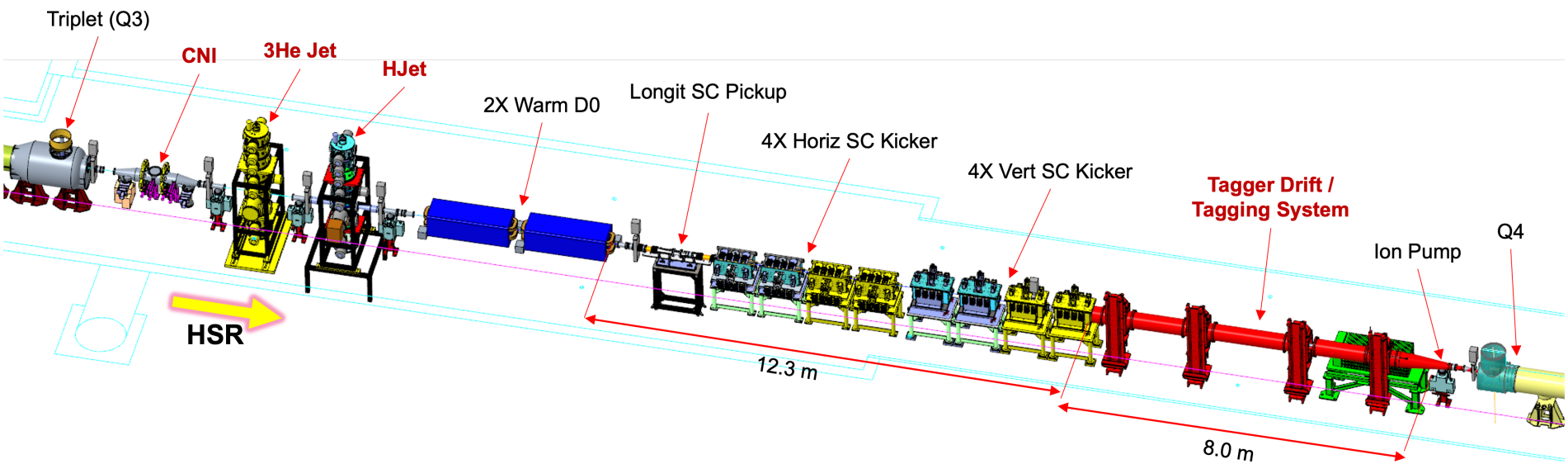

Conclusions: Critical technical developments

Solved challenges

1. EIC's tenfold increase in bunch frequency creates **electromagnetic harmonics resonantly drives hyperfine transitions** in hydrogen atoms at RHIC's HJET holding field of 120 mT. Operating at 400 mT shifts transitions safely above populated harmonics and restores robust target polarization (see F. Rathmann et al., "Eliminating beam-induced depolarizing effects in the hydrogen jet target for high-precision proton beam polarimetry at the Electron-Ion Collider," (2025), 2508.01366.).
2. **pC target heating under control:** Larger beam sizes at the pC location reduce areal power density; thermal modeling keeps $T_{\max}$ below carbon sublimation.
3. **pC wakefield mitigation:** CST studies show **dielectric holders** (e.g. Al_2O_3) with a thin 10 nm Au coating (charge control) significantly lower wake impedance vs. metallic designs.

Outlook: Ongoing developments

Ongoing developments

1. **HJET holding-field system:** engineer magnet + chamber; assess compensation for $\int B_{x,y,z}\, d\ell$; preserve vector B_x, B_y, B_z option.
2. **HJET detector system:** increased azimuthal coverage/segmentation to access (P_x, P_y, P_z); track recoils in measured guide-field (see slide 47).
3. **HJET H_2 systematics:** typical ABS H_2 at target 3 % to 4 % $\Rightarrow$ integrate QMA into BRP to accurately determine H_2 fraction;
4. **Bunch-by-bunch polarimetry:** detector/readout able to resolve 11 ns spacing (fast Si or diamond; bunch-synchronous timing).
5. **pC target thermal validation:** direct temperature measurements during beam (RHIC) and extension to IP6 conditions.
6. **pC vacuum transfer chamber:** enable target swaps without breaking ring vacuum; reduce contamination and downtime.
7. **^{3}He ABS:** cryogenic source at 1 K under development at MIT; align readiness with EIC early light-ion operations.

References I

[1] W. Haeberli, "H-jet measures beam polarization at RHIC," CERN Cour. **45N8**, 15 (2005).

[2] F. Rathmann et al., "Eliminating beam-induced depolarizing effects in the hydrogen jet target for high-precision proton beam polarimetry at the Electron-Ion Collider," (2025), 2508.01366.

[3] M. Diermaier, C. B. Jepsen, B. Kolbinger, C. Malbrunot, O. Massiczek, C. Sauerzopf, M. C. Simon, J. Zmeskal, and E. Widmann, "In-beam measurement of the hydrogen hyperfine splitting and prospects for antihydrogen spectroscopy," Nature Commun. **8**, 5749 (2017), 1610.06392.

[4] A. Airapetian, N. Akopov, Z. Akopov, M. Amarian, A. Andrus, E. Aschenauer, W. Augustyniak, R. Avakian, A. Avetissian, E. Avetissian, et al., "The hermes polarized hydrogen and deuterium gas target in the hera electron storage ring," Nuclear Instruments and Methods in Physics Research Section A: Accelerators, Spectrometers, Detectors and Associated Equipment **540**, 68 (2005), ISSN 0168-9002, URL https://www.sciencedirect.com/science/article/pii/S0168900204024167.

[5] H. Paetz gen. Schieck, *Nuclear Physics with Polarized Particles*, vol. 842 of *Lecture Notes in Physics* (Springer, Berlin, Heidelberg, 2012), ISBN 978-3-642-24225-0.

[6] N. Ramsey, *Molecular Beams* (Oxford University Press, 1956).

[7] M. E. M. Stewart, Tech. Rep. NASA/TM-2015-218987, NASA (2015), states: "graphite sublimes at 3915 K", URL https://ntrs.nasa.gov/api/citations/20150002852/downloads/20150002852.pdf.

[8] P. Thieberger, "Polarimeter target beam heating simulation version 4,", Private communication (2025), unpublished Excel-based thermal simulation code, version 27.09.2025, available upon request.

[9] M. Capiluppi, V. Carassiti, G. Ciullo, et al., "Dual H and D cavity for the PAX target polarimeter," Physics of Particles and Nuclei **45**, 283 (2014), DOI link, URL https://doi.org/10.1134/S1063779614010171.

References II

[10] N. Akchurin, J. Langland, Y. Onel, B. E. Bonner, M. D. Corcoran, J. Cranshaw, F. Nessi-Tedaldi, M. Nessi, C. Nguyen, J. B. Roberts, et al., "Analyzing power measurement of pp elastic scattering in the coulomb-nuclear interference region with the 200-gev/c polarized-proton beam at fermilab," Phys. Rev. D **48**, 3026 (1993), URL https://link.aps.org/doi/10.1103/PhysRevD.48.3026.

[11] I. G. Alekseev, A. Bravar, G. Bunce, S. Dhawan, K. O. Eyser, R. Gill, W. Haeberli, H. Huang, O. Jinnouchi, A. Kponou, et al., "Measurements of single and double spin asymmetry in *pp* elastic scattering in the cni region with a polarized atomic hydrogen gas jet target," Phys. Rev. D **79**, 094014 (2009), URL https://link.aps.org/doi/10.1103/PhysRevD.79.094014.

[12] N. H. Buttimore, "A Helium-3 polarimeter using electromagnetic interference," PoS **PSTP2013**, 057 (2013).

[13] F. Rathmann et al., "Complete angular distribution measurements of pp spin correlation parameters Axx, Ayy, and Axz and analyzing power Ay at 197.4 MeV," Phys. Rev. C **58**, 658 (1998).

[14] B. von Przewoski et al., "Proton proton analyzing power and spin correlation measurements between 250-MeV and 450-MeV at $7^\circ \leq \theta(c.m.) \leq 90^\circ$ with an internal target in a storage ring," Phys. Rev. C **58**, 1897 (1998).

[15] B. von Przewoski, H. O. Meyer, P. V. Pancella, S. F. Pate, R. E. Pollock, T. Rinckel, F. Sperisen, J. Sowinski, W. Haeberli, W. K. Pitts, et al., "Absolute measurement of the p+p analyzing power at 183 mev," Phys. Rev. C **44**, 44 (1991), URL https://link.aps.org/doi/10.1103/PhysRevC.44.44.

[16] G. Plattner and A. Bacher, "Absolute calibration of spin-$\frac{1}{2}$ polarization," Physics Letters B **36**, 211 (1971), ISSN 0370-2693, URL https://www.sciencedirect.com/science/article/pii/0370269371900712.

References III

[17] R. E. Pollock, W. A. Dezarn, M. Dzemidzic, J. Doskow, J. G. Hardie, H. O. Meyer, B. v. Przewoski, T. Rinckel, F. Sperisen, W. Haeberli, et al., "Calibration of the polarization of a beam of arbitrary energy in a storage ring," Phys. Rev. E **55**, 7606 (1997), URL https://link.aps.org/doi/10.1103/PhysRevE.55.7606.

[18] B. v. Przewoski et al., "Analyzing powers and spin correlation coefficients for $p + d$ elastic scattering at 135 and 200 MeV," Phys. Rev. C **74**, 064003 (2006), URL http://link.aps.org/doi/10.1103/PhysRevC.74.064003.

[19] P. Blümler and H. Soltner, "Practical Concepts for Design, Construction and Application of Halbach Magnets in Magnetic Resonance," Applied Magnetic Resonance **54**, 1701 (2023), ISSN 1613-7507, URL https://doi.org/10.1007/s00723-023-01602-2.

[20] H. Soltner and P. Blümler, "Dipolar halbach magnet stacks made from identically shaped permanent magnets for magnetic resonance," Concepts in Magnetic Resonance Part A **36A**, 211 (2010), https://onlinelibrary.wiley.com/doi/pdf/10.1002/cmr.a.20165, URL https://onlinelibrary.wiley.com/doi/abs/10.1002/cmr.a.20165.

[21] H. Raich and P. Blümler, "Design and construction of a dipolar halbach array with a homogeneous field from identical bar magnets: Nmr mandhalas," Concepts in Magnetic Resonance Part B: Magnetic Resonance Engineering **23B**, 16 (2004), https://onlinelibrary.wiley.com/doi/pdf/10.1002/cmr.b.20018, URL https://onlinelibrary.wiley.com/doi/abs/10.1002/cmr.b.20018.

[22] K. Abe, K. Tadakuma, and R. Tadakuma, "Abenics: Active ball joint mechanism with three-dof based on spherical gear meshings," IEEE Transactions on Robotics **37**, 1806 (2021).

[23] J. Abrahamson, "Graphite sublimation temperatures, carbon arcs and crystallite erosion," Carbon **12**, 111 (1974), concludes one-atmosphere sublimation temperature lies between 3895 and 4020 K.

References IV

[24] M. Planck, *The Theory of Heat Radiation* (P. Blakiston's Son & Co., 1914).

[25] L. Brewer, P. W. Gilles, and F. A. Jenkins, "The vapor pressure and heat of sublimation of graphite," The Journal of Chemical Physics **16**, 797 (1948).

[26] J. R. Haines and C. C. Tsai, Tech. Rep. ORNL/TM-2002/27, Oak Ridge National Laboratory, Oak Ridge, TN (2002), summarizes literature vapor-pressure fits for graphite and maps them to UHV erosion rates via the Hertz–Knudsen relation., URL `https://info.ornl.gov/sites/publications/Files/Pub57715.pdf`.

[27] J. F. O'Hanlon, *A User's Guide to Vacuum Technology* (John Wiley & Sons, Hoboken, NJ, 2003), 3rd ed.

[28] C. Weidemann, F. Rathmann, H. J. Stein, B. Lorentz, Z. Bagdasarian, L. Barion, S. Barsov, U. Bechstedt, S. Bertelli, D. Chiladze, et al., "Toward polarized antiprotons: Machine development for spin-filtering experiments," Phys. Rev. ST Accel. Beams **18**, 020101 (2015), URL `http://link.aps.org/doi/10.1103/PhysRevSTAB.18.020101`.

Spare slides

Coulomb-Nuclear interference I

Need for calibration

- Asymmetry from CNI region constitutes basis of RHIC high-energy (absolute) polarimeters
  - derived from same EM amplitude that generates anomalous magnetic moment

$$\mu_p = g_p \frac{e\hbar}{2m_p} = g_p \mu_N, \quad g_p \approx 5.585$$
$$g_p - 2 \approx 3.585 \Rightarrow \mu_p^{\text{anomalous}} \approx 1.792\,\mu_N \tag{10}$$

  - E704 at Fermilab used 200 GeV/c $\vec{p}$ from hyperon decay to detect asymmetry in scattering from H target [10]. Largest $A_y \approx 0.04$ with large statistical errors.
  - Meanwhile, accurate measurements of A_y are available from RHIC [11]
- Asymmetry measurements involve normalization uncertainties and calculations of A_y are subject to uncertainties in amplitudes of strong interaction. **Therefore, accurate calibration of reaction required.**

Coulomb-Nuclear interference II

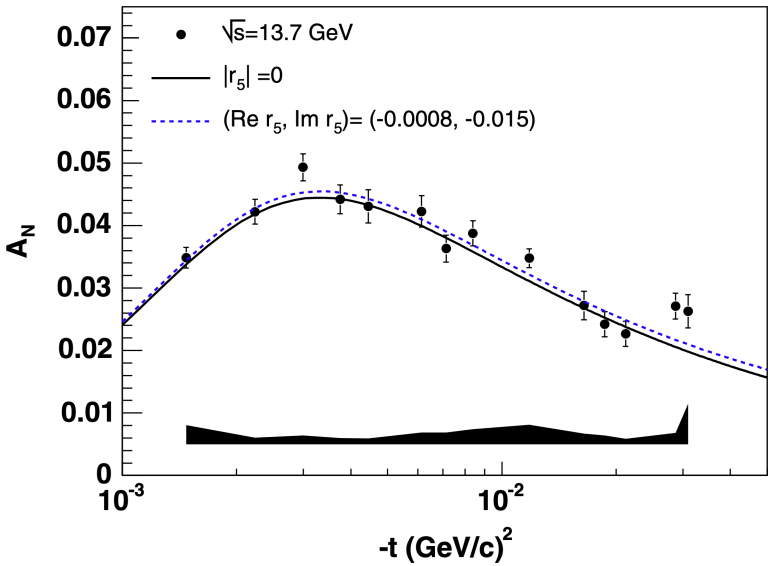

Measured A_N from RHIC in the CNI region at $\sqrt{s} = 6.8\,\text{GeV}$ ($E_{\text{lab}} = 23.7\,\text{GeV}$) [11].

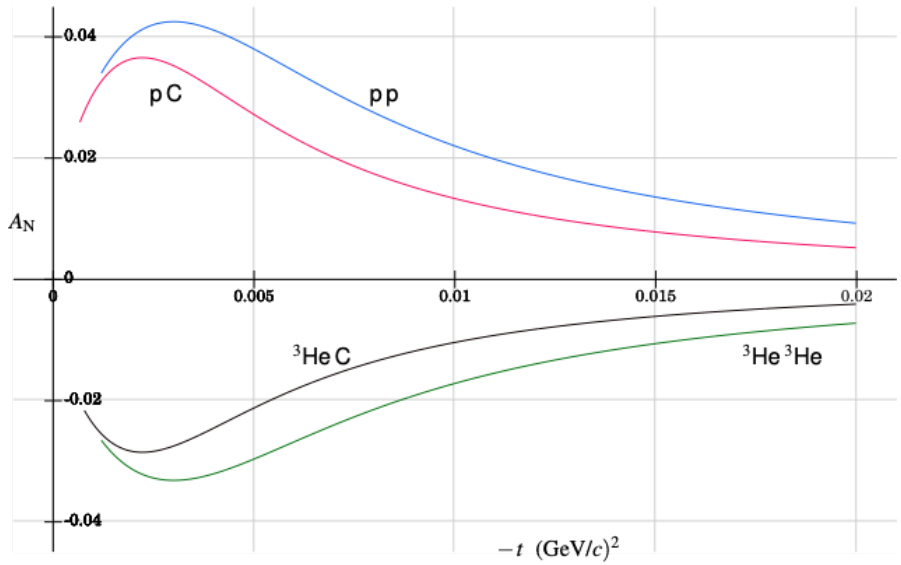

Calculation of A_y in the CNI region by Nigel Buttimore [12].

Critical field for hydrogen hyperfine splitting I

Zeeman region:

- magnetic flux density at which energy separation between different hyperfine levels becomes comparable to Zeeman splitting.
- referred to as *critical magnetic field* or *Breit-Rabi field* B_c
- Breit-Rabi formula (energy levels of hydrogen atom in external magnetic field:

$$E_{F,m_F} = -\frac{E_{\text{hfs}}}{2(2I+1)} + g_J \mu_B m_J B \pm \frac{E_{\text{hfs}}}{2}\sqrt{1 + \frac{2m_F x}{F} + x^2}\,, \text{where} \qquad (11)$$

- E_{hfs} is hyperfine splitting energy
- I is nuclear spin (for H, $I = \frac{1}{2}$)
- g_J is Landé g-factor
- μ_B is Bohr magneton
- m_J is magnetic quantum number
- m_F is total angular momentum quantum number
- $x = \frac{g_J \mu_B B}{E_{\text{hfs}}}$
- $F = I + J$ is total angular momentum (for H, $J = \frac{1}{2}$)

Critical field for hydrogen hyperfine splitting II

For H:

- hyperfine splitting energy E_{hfs} (1420 MHz):

$$E_{\mathrm{hfs}} \approx 5.874 \times 10^{-6}\,\mathrm{eV} \tag{12}$$

- Critical field B_c is when Zeeman energy $g_J \mu_B B$ is comparable to E_{hfs}. With $g_J \mu_B B_c \approx E_{\mathrm{hfs}}$, we get:

$$B_c \approx \frac{E_{\mathrm{hfs}}}{g_J \mu_B} \tag{13}$$

- For H, $g_J \approx 2$ (approximately for electron), and $\mu_B \approx 5.788 \times 10^{-5}\,\mathrm{eV/T}$. Thus,

$$B_c \approx \frac{5.874 \times 10^{-6}\,\mathrm{eV}}{2 \times 5.788 \times 10^{-5}\,\mathrm{eV/T}} \approx 50.7\,\mathrm{mT} \tag{14}$$

Concept for magnetic guide field for HJET at EIC

But first ...

Spin-dependent *pp* elastic cross section (spin 1/2 + spin 1/2)

With polarized beam $\vec{P}$ and polarized target $\vec{Q}$, all components of $\vec{P}$ can be determined from spin-dependent cross section, as shown in Table below [13, 14]:

$$\begin{aligned}\sigma/\sigma_0 = 1 &+ A_y \left[(P_y + Q_y)\cos\phi - (P_x + Q_x)\sin\phi\right] \\ &+ A_{xx}\left[P_x Q_x \cos^2\phi + P_y Q_y \sin^2\phi + (P_x Q_y + P_y Q_x)\sin\phi\cos\phi\right] \\ &+ A_{yy}\left[P_x Q_x \sin^2\phi + P_y Q_y \cos^2\phi - (P_x Q_y + P_y Q_x)\sin\phi\cos\phi\right] \\ &+ A_{xz}\left[(P_x Q_z + P_z Q_x)\cos\phi + (P_y Q_z + P_z Q_y)\sin\phi\right] + A_{zz} P_z Q_z\end{aligned}$$

- Full angular distributions of all A_{ik}'s were determined.
- Single input: $A_y = 0.2122 \pm 0.0017$ at $\theta_{\text{lab}} = 8.64^\circ \pm 0.07^\circ$ [15], known from $A_y = 1$ point in $p + {}^{12}\text{C}$ elastic scattering [16].

Most importantly in context

- determination of beam $\vec{P} = (P_x, P_y, P_z)$ and target $\vec{Q} = (Q_x, Q_y, Q_z)$, as well as non-flipping components possible (slide 48)

Polarization of beam $\vec{P}$ and target $\vec{Q}$ [13, 14]

	$\pm x$		$\pm y$		$\pm z$	
	PRE	POST	PRE	POST	PRE	POST
P_x	0.0052(47)	0.0089(44)	0.0052(47)	0.0089(44)	0.0052(47)	0.0089(44)
P_y [a]	**0.5801(34)**	**0.5425(32)**	**0.5802(34)**	**0.5417(32)**	**0.5765(34)**	**0.5447(32)**
P_z	−0.0021(47)	0.0003(44)	−0.0021(47)	0.0003(44)	−0.0021(47)	0.0003(44)
Q_x	**0.7401(59)**	**0.7394(56)**	−0.0039(59)	0.0039(56)	−0.0071(23)	−0.0052(23)
Q_y	0.0111(59)	0.0039(56)	**0.7400(59)**	**0.7406(56)**	−0.0055(59)	−0.0034(56)
Q_z	0.0158(60)	0.0240(60)	−0.0174(61)	−0.0121(61)	**0.7401(42)** [b]	**0.7400(40)** [b]
S_{P_y}	−0.0008(18)	−0.0005(17)	−0.0008(18)	0.0005(17)	−0.0008(18)	0.0005(17)
S_{Q_x}	0.0017(23)	−0.0007(23)	−0.0040(23)	−0.0031(23)	−0.0043(23)	−0.0024(23)
S_{Q_z}	−0.0091(82)	−0.0162(82)	−0.0177(82)	−0.0197(82)	0.0013(82)	−0.0086(82)

- Beam polarization export/calibration to arbitrary energy [17]
  - PRE ≡ b (197.4 MeV)
  - Export ≡ c (399.1 MeV)
  - POST ≡ d (197.4 MeV)

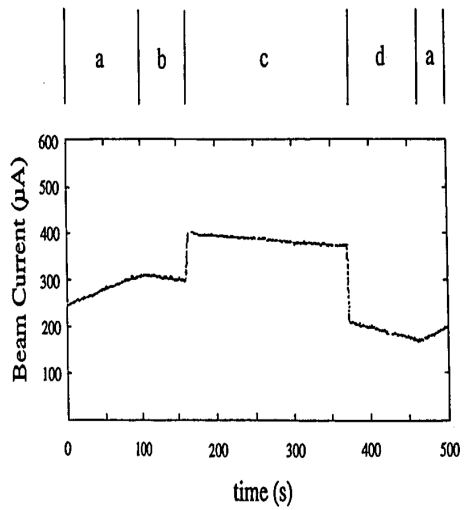

Spin-dependent *pp* elastic cross section

The above is relevant for two reasons

1. The spin-dependence of $\vec{p}\vec{p}$ elastic scattering allows to reconstruct angular distributions of all (in that case five) polarization observables.
2. With suitable magnetic guide field, target polarization $\vec{Q}$ can be oriented along any direction, for instance along x, so that $\vec{Q} = Q \cdot \vec{e}_x = \vec{Q}_x$
   - Absolute value of target polarization Q determined by BRP

Two things needed to port HJET from RHIC to EIC with $\frac{\Delta P}{P} \leq 1\%$

1. Substantially stronger holding field of $|\vec{B}| \approx 300$ to 350 mT than at RHIC
2. Detector capable to pick up azimuthal asymmetries $\propto \sin\phi$ and $\propto \sin 2\phi$ (slide 50)
   - foresee proper detector symmetry to provide $\vec{d}\vec{d}$ beam absolute polarimetry, i.e., beyond $\propto \sin 2\phi$.

Detector symmetry required to accomplish the task

For spin $\frac{1}{2}$ + spin $\frac{1}{2}$ scattering, suitable geometry below shows pattern of detected azimuthal angles [13].

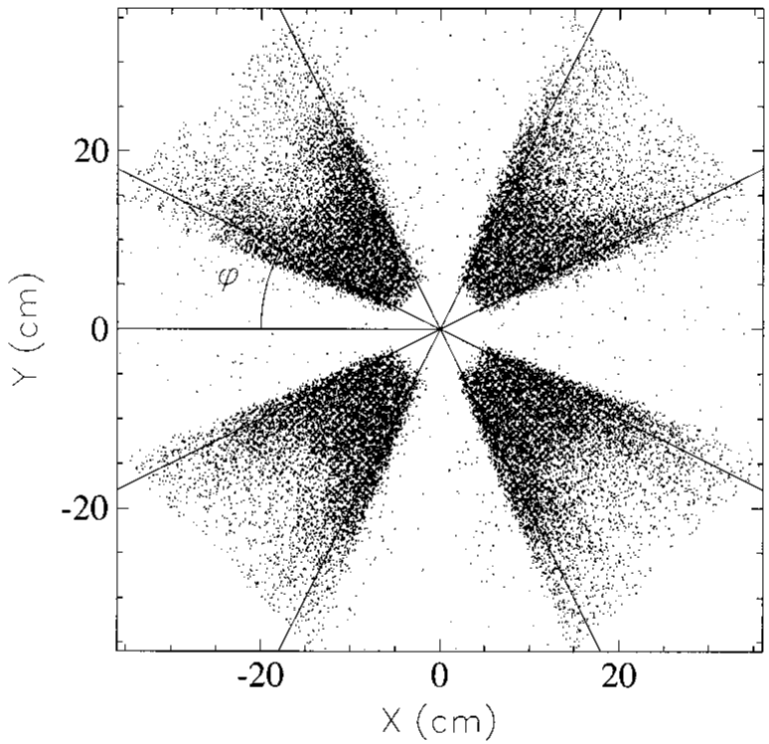

For spin $\frac{1}{2}$ + spin 1 scattering, a higher segmentation is needed, because besides $\sin\phi$ and $\sin 2\phi$, also terms $\sin 3\phi, \ldots$ contribute to asymmetries [18].

Holding field system for $|\vec{B}| \approx 0.3\,\mathrm{T}$ with $\vec{B} \parallel \vec{e}_{x,y,z}$

Work in part together with Helmut Soltner (FZJ, Germany)

Motivation:

- Reconcile strong magnetic holding field with open detector geometry to determine, e.g., all spin components of beam polarization $\vec{P} = (P_x, P_y, P_z)$
- Exploit magnetic moments $\vec{m}$ of homogeneously magnetized spheres [19–21]
- Invert $\vec{m}$ in vacuum to reverse $\vec{B}(O)$
- Reorient $\vec{m}$'s to generate $\vec{B}(O) \parallel \vec{e}_{x,y,z}$

Consider two sets of frames

- Beam meets atoms at (O)
  - Set 1: $100\,\mathrm{mm}_x \times 100\,\mathrm{mm}_y \times 40\,\mathrm{mm}_z$
  - Set 2: $100\,\mathrm{mm}_x \times 100\,\mathrm{mm}_y \times 110\,\mathrm{mm}_z$
  - 8 magnetized spheres in corners of frames:
  - NeFeB magnets provide remanence of $B_r = 1.49 - 1.55\,\mathrm{T}$ (type N58)
  - Radius $r = 30\,\mathrm{mm}$

Holding field system: Calculation

- Flux density vector as fct of $\vec{m}$ in space

$$\vec{B}(\vec{r}) = \frac{\mu_0}{4\pi}\left[\frac{3\left(\vec{m}\cdot\hat{R}\right)\hat{R}-\vec{m}}{|R|^3}\right] \quad (15)$$

$$\vec{R} = \vec{r} - \vec{r}_0, \hat{R} = \frac{\vec{R}}{|R|}$$

- Optimize orientation of $\vec{m}$'s to maximize $\vec{B}(O)$ along $\vec{e}_x$, $\vec{e}_y$, or $\vec{e}_z$
  - maximize dot product $\vec{m}\cdot\hat{R}$, set $m_y = 0$ to obtain, e.g., max. B_y

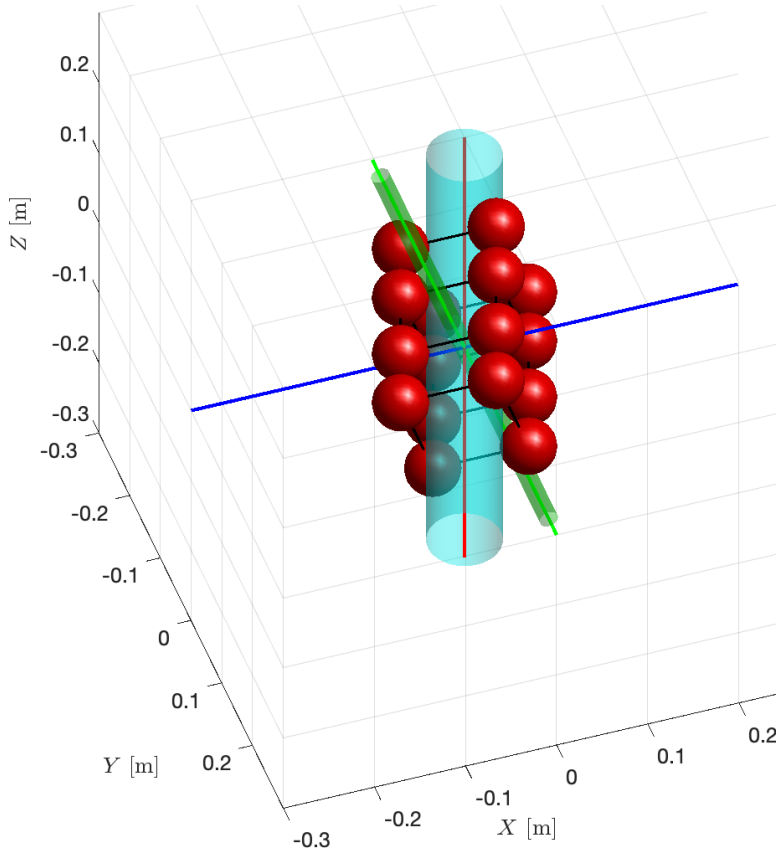

16 spherical magnetic dipoles

- atomic beam $\parallel \vec{e}_y$
- ion beam $\parallel \vec{e}_z$

Component $B_x(O)$ using two sets of $\vec{m}$'s

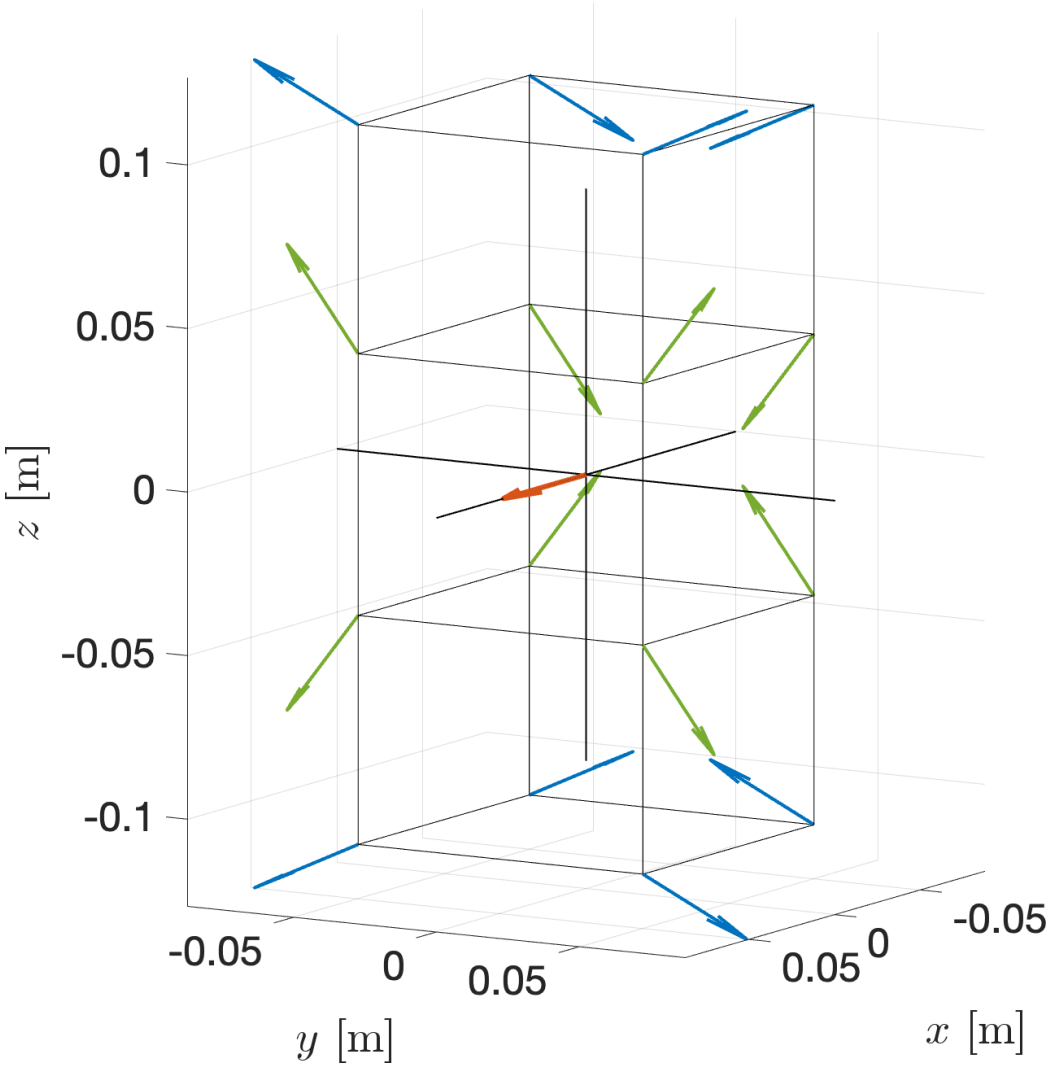

$$B_x: \begin{pmatrix} 0.3224 \\ 0 \\ 0 \end{pmatrix} \text{T}$$

Component $B_y(O)$ using two sets of $\vec{m}$'s

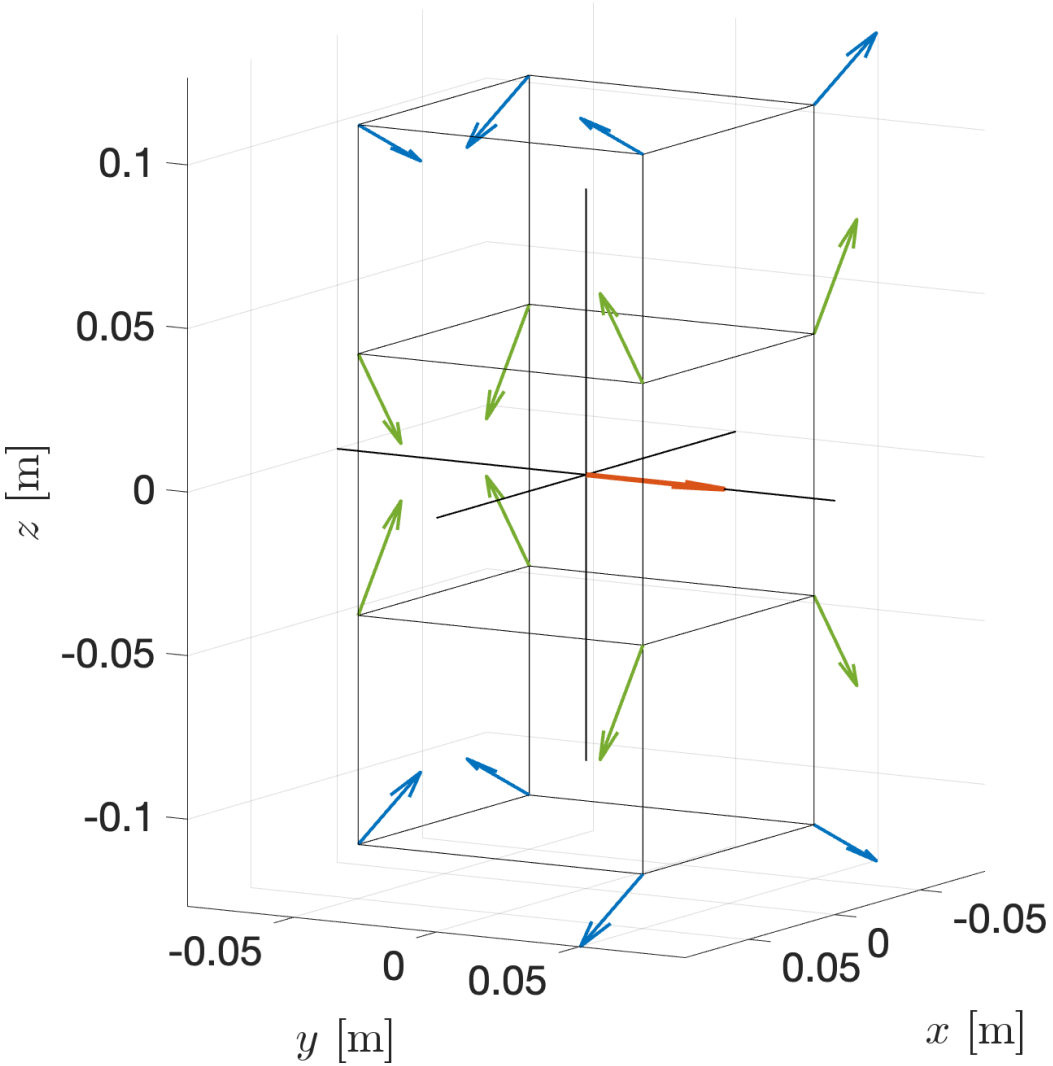

$$B_y: \begin{pmatrix} 0 \\ 0.3224 \\ 0 \end{pmatrix} \text{ T},$$

Component $B_z(O)$ using two sets of $\vec{m}$'s

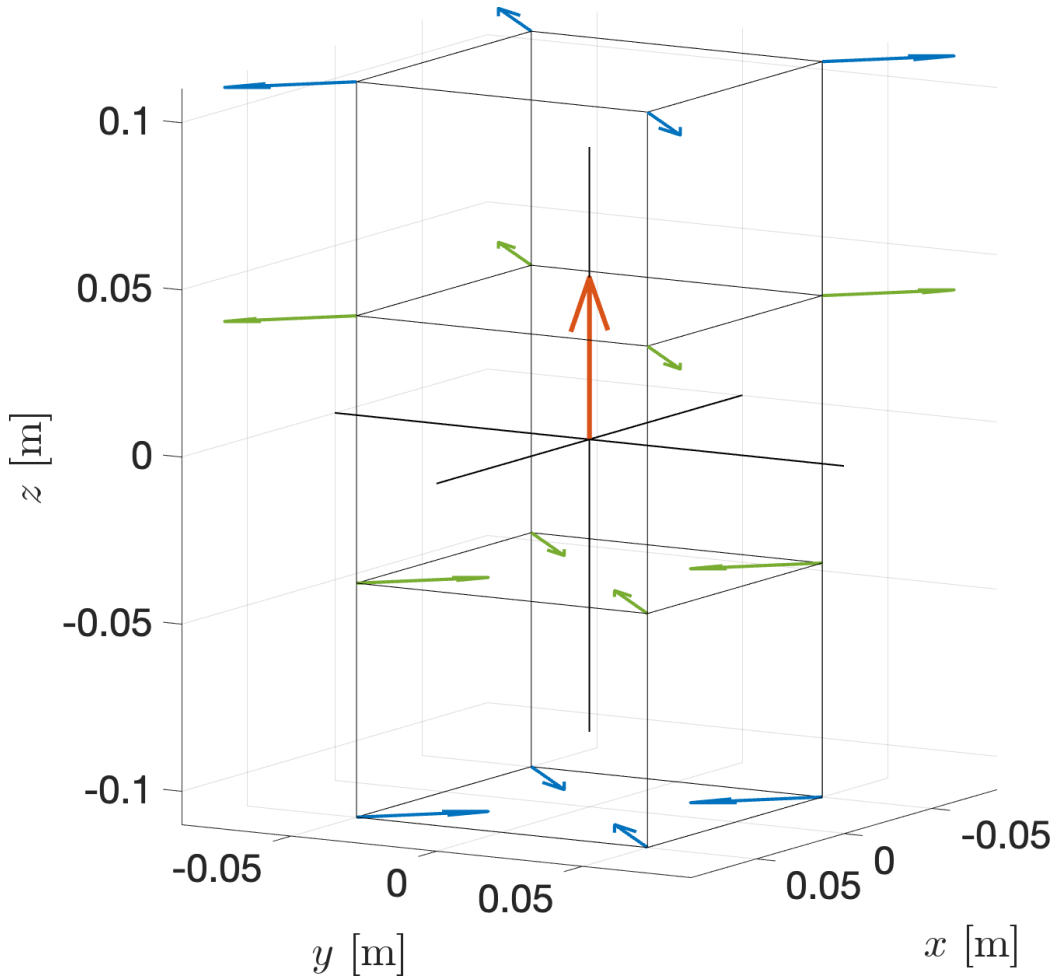

$$B_z: \begin{pmatrix} 0 \\ 0 \\ 0.3227 \end{pmatrix} \text{T}$$

Technical realization

LDRD C application approved

With properly rotated spheres

- Setup allows for azimuthally symmetric detector setup with acceptance $\Delta\phi \approx \pm 20^\circ$ at $\phi = 45$, 135, 225, and 315°
  - Slides 50 and 48 show azimuthal acceptance could look like
- **Technical challenges:**
  1. Accurate 3D reorientation of magnetized spheres[a] in vacuum [22]
  2. Vacuum compatible coating, like Ni, or stainless steel covers to prevent H and H_2 from deteriorating NeFeB
  3. **First Step: build a lab test setup and verify concept is technically sound**
  4. Forces and torques appear manageable (next slides)

[a] https://www.youtube.com/watch?v=hhDdfiRCQS4

Force and torque between two dipoles $\vec{m}_1$ and $\vec{m}_2$ I

Potential energy of magnetic dipole

$$U = -\vec{m} \cdot \vec{B}$$
$$\vec{F} = -\vec{\nabla} U \quad \rightarrow \quad F_{12} = \vec{\nabla}\left(\vec{m}_2 \cdot \vec{B}_1\right) \tag{16}$$

- $\vec{B}_1$ is flux density produced by $\vec{m}_1$ at location of $\vec{m}_2$.

Force:

$$\vec{F}_{12}(\vec{r}_{12}, \vec{m}_1, \vec{m}_2) = \frac{3\mu_0}{4\pi r_{12}^4}\Big[\vec{m}_2\left(\vec{m}_1 \cdot \vec{e}_{12}\right) + \vec{m}_1\left(\vec{m}_2 \cdot \vec{e}_{12}\right) + \vec{e}_{12}\left(\vec{m}_1 \cdot \vec{m}_2\right) - 5\vec{e}_{12}\left(\vec{m}_1 \cdot \vec{e}_{12}\right)\left(\vec{m}_2 \cdot \vec{e}_{12}\right)\Big] \tag{17}$$

- $\vec{r}_{12}$ is vector between $\vec{m}_1$ and $\vec{m}_2$, $\vec{e}_{12} = \frac{\vec{r}_{12}}{|r_{12}|}$.

Torque

$$\vec{\tau} = \vec{m}_2 \times \vec{B}_1 \tag{18}$$

Force and torque between two dipoles $\vec{m}_1$ and $\vec{m}_2$ II

Examples: $\vec{m}_1 \perp \vec{m}_2$

1. Spheres touch:

$$r_{12} = 0.06\,\mathrm{m} \quad \vec{F}_{12} = -417\,\mathrm{N} \quad \tau_{12} = 8.3\,\mathrm{Nm} \tag{19}$$

2. System assembled:

$$r_{12} \geq 0.07\,\mathrm{m} \quad \vec{F}_{12} \leq -225\,\mathrm{N} \quad \tau_{12} = 5.2\,\mathrm{Nm} \tag{20}$$

Flux density of system in 3D

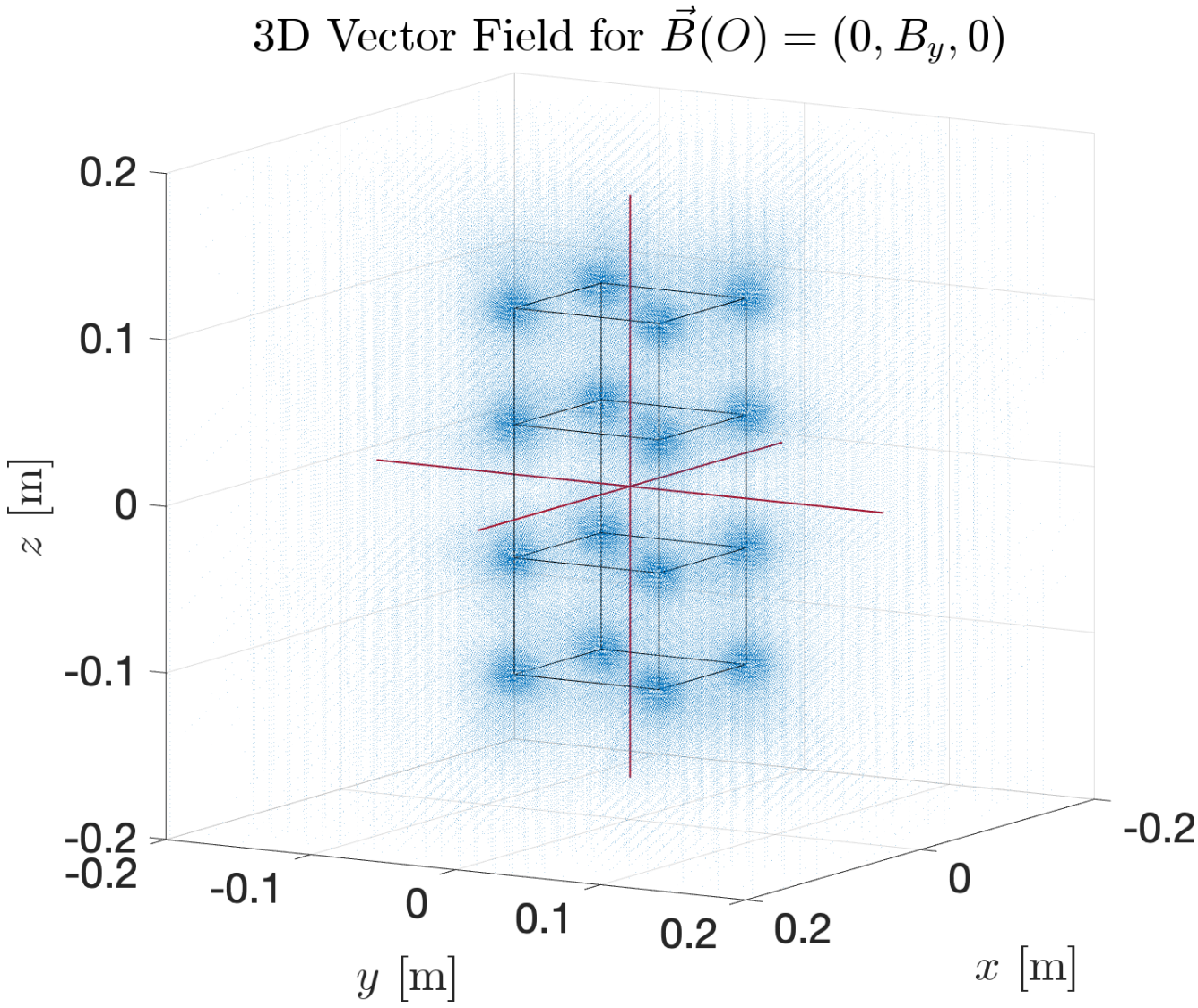

No zero crossings along axes

$\vec{B}(O) \parallel \vec{e}_x$

$\vec{B}(O) \parallel \vec{e}_y$

$\vec{B}(O) \parallel \vec{e}_z$

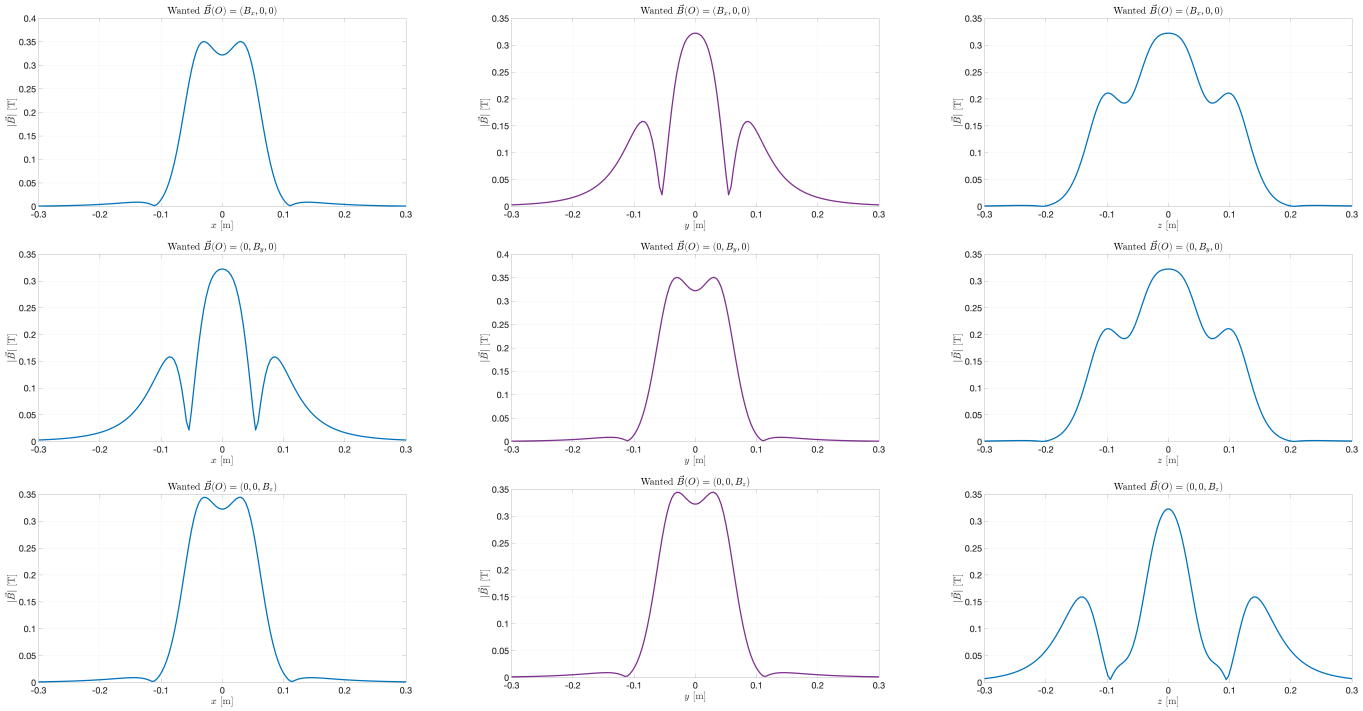

x y z

- No zero crossing of magnetic field along vertical jet (y) axis
- $B_y^{\min} \approx 1.9\,\mathrm{mT}$ sufficient to avoid **Majorana depolarization**
- Field integrals along beam (z) axis

$\vec{B}(O)$	$\parallel \vec{e}_x$	$\parallel \vec{e}_y$	$\parallel \vec{e}_z$
$\int \lvert\vec{B}\rvert \mathrm{d}z$	0.0667 Tm	0.0667 Tm	0.0546 Tm

Direct measurement of temperature of carbon targets

Work with Frank Rathmann, Prashanth Shanmuganathan, Oleg Eyser, Haixin Huang, Dannie Steskie, Thomas Tsang, and George Mahler

- Carbon fiber targets of RHIC polarimeters do not reach carbon sublimation temperature[a] of $T_{\text{sub}} = 3915\,\text{K}$ [7]:
  - **targets survive proton bombardment** at RHIC.
  - Observation aligns coarsely with energy loss calculations by Peter Thieberger (BNL) using appropriate beam sizes at the interaction point.
- Direct temperature measurement of carbon targets remains crucial goal
  - Black-body radiation [24] as a method to determine temperature by analyzing the emitted light spectrum.
- **APEX measurement approved for run 25**
  - more details on this investigations on slides slides 65 – 69

[a] Ref. [23] gives sublimation temperatures at one atmosphere pressure of 3895 K to 4020 K.

Carbon sublimation (Hertz–Knudsen) I

Thermodynamics vs. operations

- At $\sim$1 atm, carbon has no melt; it **sublimes** near $T_{\text{sub}} \approx 3915\,\text{K}$ (graphite) [23].
- In high/ultra-high vacuum the **vapor pressure** $P_{\text{vap}}(T)$ controls the mass loss; practical ceilings for longevity are typically $\lesssim 3200\,\text{K}$ to $3500\,\text{K}$ depending on geometry/surface condition and allowed erosion.
- Thin ribbons/films (large area, edge density) show higher evaporation rates at the same T than bulk graphite; coatings change emissivity and kinetics.

Carbon sublimation (Hertz–Knudsen) II

Hertz-Knudsen flux (vacuum evaporation/sublimation)

$$J = \alpha \frac{P_{\text{vap}}(T) - P_{\text{amb}}}{\sqrt{2\pi\, m\, k_{\text{B}}\, T}}, \qquad \frac{\dot{m}}{A} = J\, m. \tag{21}$$

- J [$\text{m}^{-2}\,\text{s}^{-1}$]: flux (particles per unit area per unit time).
- α [1]: evaporation/accommodation coefficient ($0 \leq \alpha \leq 1$).
- $P_{\text{vap}}(T)$ [Pa]: equilibrium vapor pressure at surface temperature T.
- P_{amb} [Pa]: ambient partial pressure of the same vapor species.
- m [kg]: molecular mass of the evaporating species (e.g., C or C_2).
- k_{B} [$\text{J}\,\text{K}^{-1}$]: Boltzmann constant.
- T [K]: absolute surface temperature.
- $\dot{m}/A$ [$\text{kg}\,\text{m}^{-2}\,\text{s}^{-1}$]: mass loss rate per unit surface area .

Carbon sublimation (Hertz–Knudsen) III

When $P_{\text{amb}} \approx 0$ (high/ultra-high vacuum)

$$\frac{\dot{m}}{A} \approx \alpha \frac{m\, P_{\text{vap}}(T)}{\sqrt{2\pi\, m\, k_{\text{B}}\, T}} = \alpha \frac{\sqrt{m}\, P_{\text{vap}}(T)}{\sqrt{2\pi\, k_{\text{B}}\, T}}\,. \tag{22}$$

- For $P_{\text{vap}}(T)$ and usage in UHV, see [25–27].

Experimental setup

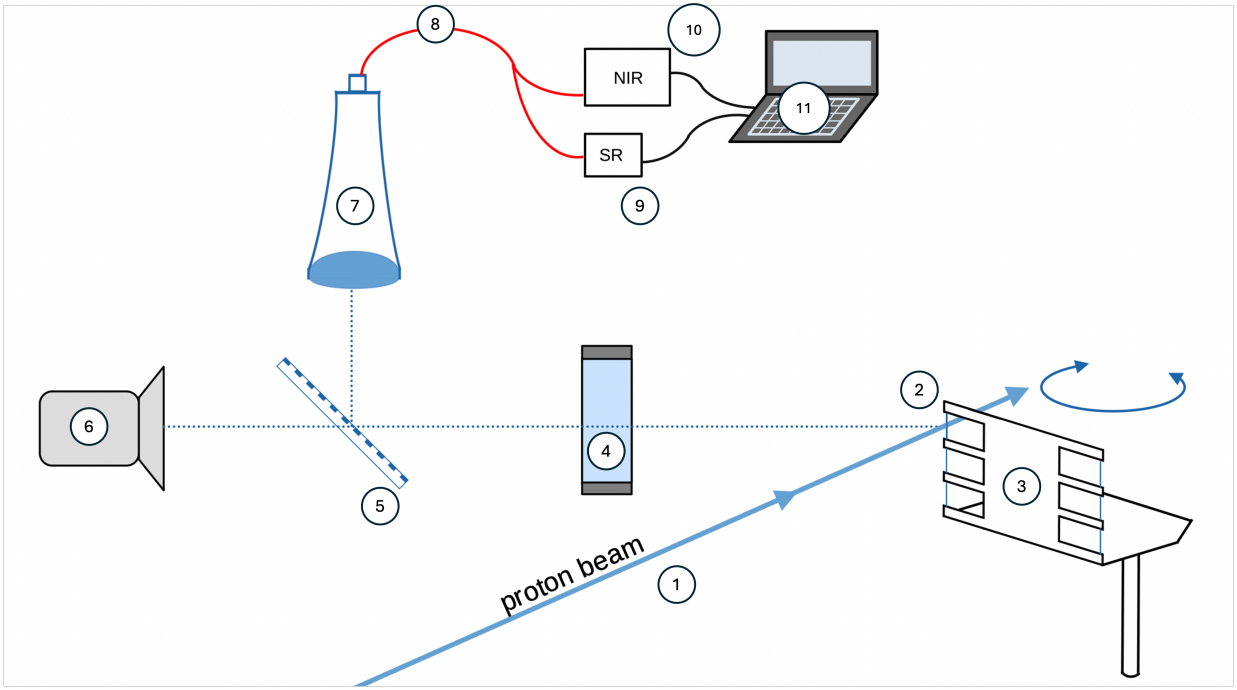

1. proton beam
2. fiber target
3. target holder
4. fused-silica viewport
5. semi-transparent polka-dot mirror
6. optical camera
7. collimator lens
8. fiber splitter (VIS and IR)
9. spectrometer VIS (SR)
10. spectrometer IR (NIR)
11. spectral analysis ($\lambda = 200 - 2200\,\text{nm}$)

Black body radiation

Ideally, one would measure:

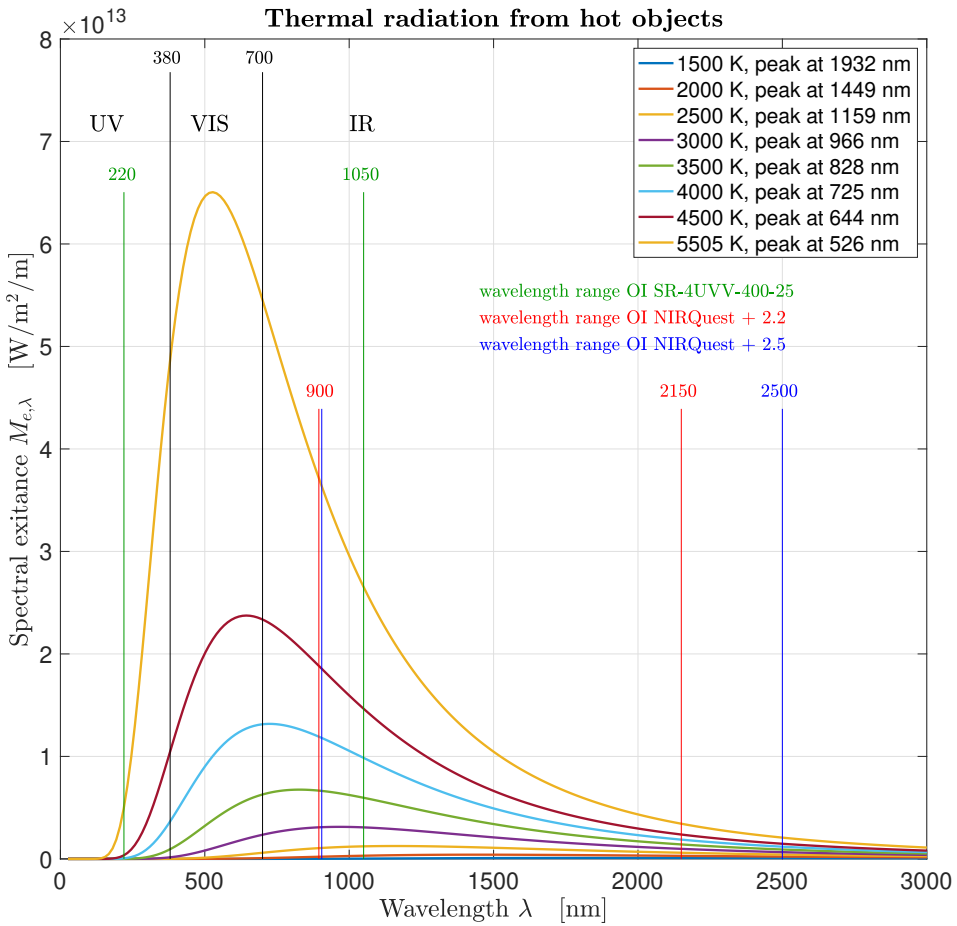

wavelength-dependent attenuation in

- fused-silica viewport
- collimator lens
- 100 m glass fibers from IP12 to spectrometers

Lab test measurement using IR light source

Experimental setup

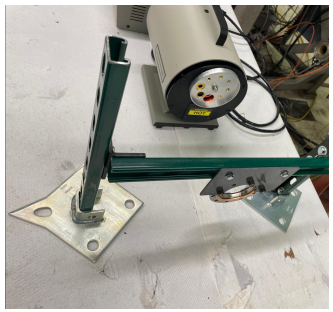

Black body radiation using oven at 1463 K

- SR spectrometer: 200 to 900 nm
- NIR spectrometer: 900 to 2100 nm
- Light path includes fiber splitter and 100 m glass fibers
- Measured spectrum compared to blackbody radiation spectra at 1463 K, 1263 K, and 1663 K

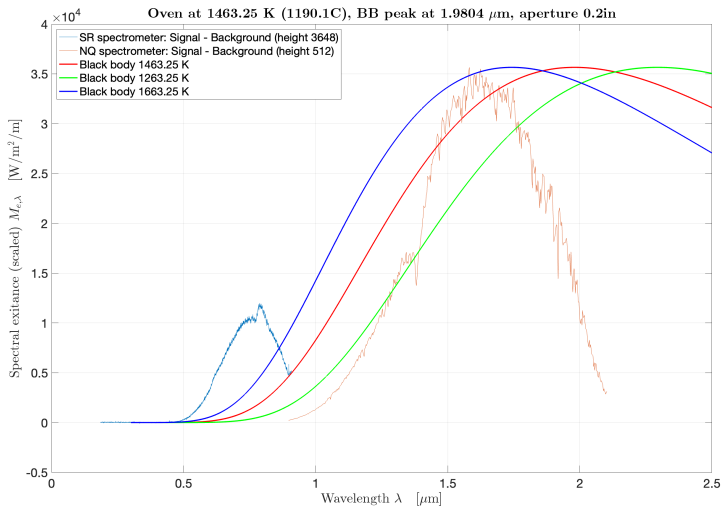

Test measurements using C targets at IP4

- In 2024, equipment/components arrived late, thus optimal alignment of light collection system at IP4 was not possible.
- We observe a clear signal, however, the light intensity is low because we don't aim at the brightest spot on the target
- For the same reason, the temperature we observe is only around 1400 K, about half of what we would expect

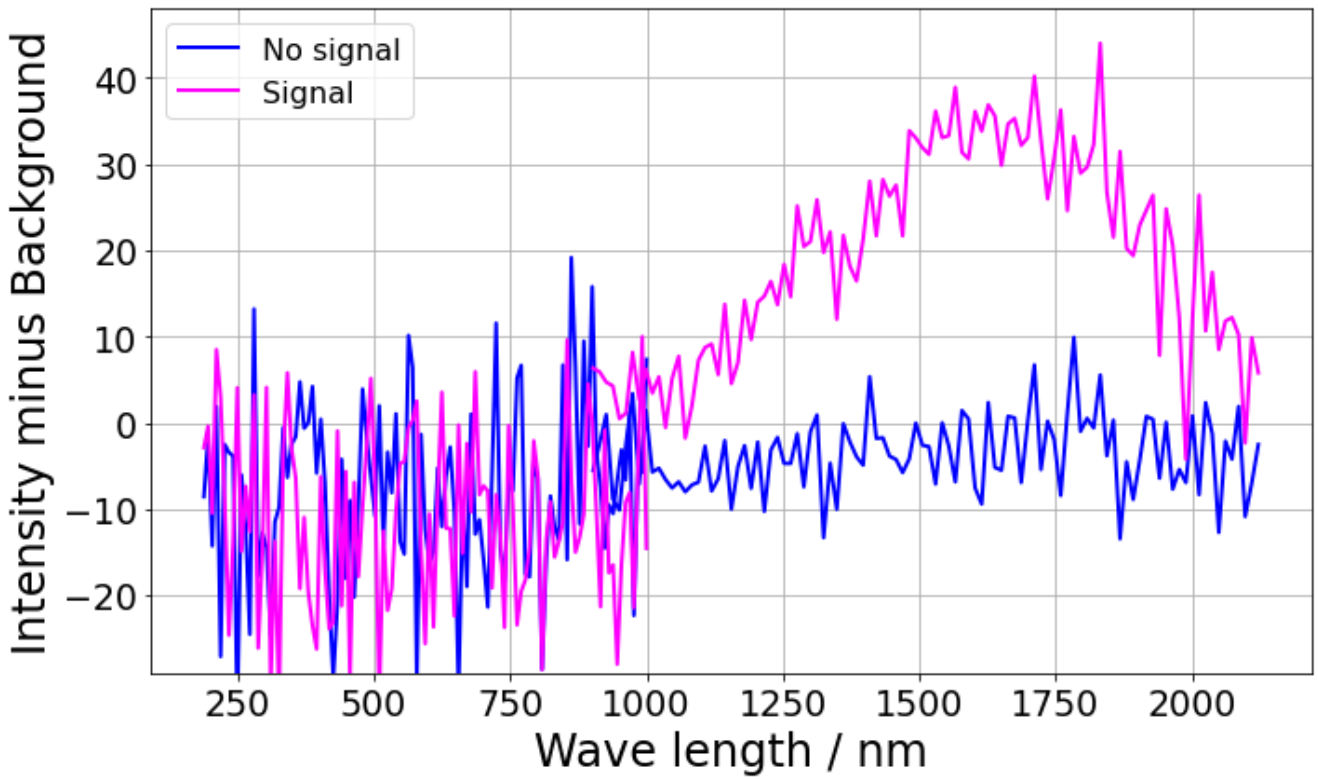

APEX proposal

Goals for run 25

- **Ensure full understanding of energy loss/heating of carbon polarimetry fiber targets by high energy proton beam, in particular for EIC**
- Light collection system was installed and operated already during run 24
  - As CNI chamber was already sealed off/pumped down when all components were available, light collection system could not be properly aligned
- **Improve alignment before ring closes, repeat measurement in run 25**
  1. Our APEX requires dedicated time only in case no proton beam available in run 25. With 100 GeV stored protons, we can run parasitically.
  2. Need 100 GeV protons in blue with max. number of bunches stored
  3. With beam on flattop, a single fill of the machine should be sufficient:
     - Sweep one target back and forth through the beam, then do another one, and so on. No need to wait for target cool down.
     - Will use four targets in blue, two horizontal ones and two vertical ones.
  4. 2h sweeping targets back and forth sufficient to achieve goals
  5. In case something goes wrong with 3. and 4., we need a 2^{nd} fill

^{3}He jet target thickness I

- **Given**
  - Flux $I = 1 \times 10^{14}\,\mathrm{s}^{-1}$, temperature $T = 1.3\,\mathrm{K}$, $m_{^3\mathrm{He}} \approx 3.016\,\mathrm{u}$.
  - Jet diameter $D = 1.0\,\mathrm{cm}$ (uniform profile) $\Rightarrow$ area $A = \pi(D/2)^2$.
  - Ion beam fully inside jet; line length along beam $L = 1\,\mathrm{cm}$.
  - Mean speed (Maxwell): $\bar{v} = \sqrt{\dfrac{8 k_B T}{\pi m}}$.
  - Volume density [cm^{-3}]: $\rho = \dfrac{I}{\bar{v}\, A}$.
  - Areal density (target thickness): $d_t = \displaystyle\int \rho \, \mathrm{d}\ell \approx \rho L = \frac{I\, L}{\bar{v}\, A}$.
  - $\bar{v} \approx 9.6 \times 10^3\,\mathrm{cm\,s}^{-1}$ (for ^{3}He at 1.3 K).
  - $A = \pi(0.5)^2\ \mathrm{cm}^2 \approx 7.85 \times 10^{-1}\,\mathrm{cm}^2$.
- **Areal density of ^{3}He jet**

$$d_t = \rho\, L \approx 1.3 \times 10^{10}\ \mathrm{atoms\,cm}^{-2}. \tag{23}$$

  - *Scaling* $d_t \propto IL/(A\sqrt{T})$ with $A \propto D^2$.

^{3}He jet target thickness II

Storage cell (molecular–flow model [28]), cooled at $T = 77\,\mathrm{K}$

- **Geometry** (all $d = 1.0\,\mathrm{cm}$):
  - Injection tube: $\ell_{\mathrm{inj}} = 10\,\mathrm{cm}$.
  - Beam tubes: $\ell_{\mathrm{up}} = \ell_{\mathrm{down}} = 30\,\mathrm{cm}$.
  - Cell length along beam: $\ell_t = 60\,\mathrm{cm}$.
- **Molecular–flow tube conductance** [28, Eq. (13)]:

$$C_{\mathrm{tube}} \;=\; 3.81\,\sqrt{\frac{T}{M}}\;\frac{d^3}{\ell\left[\,1 + 1.33\,(d/\ell)\,\right]}. \tag{24}$$

  - C_{tube} in $\mathrm{L\,s^{-1}}$, d, ℓ in cm, T in K, M in $\mathrm{g\,mol^{-1}}$.
- **Total cell conductance** (for ^{3}He, $T = 77\,\mathrm{K}$):
  - Using the three–tube geometry above and $M = 3.016\,\mathrm{g/mol}$,

$$C_{\mathrm{tot}} \;\approx\; 2.92\,\mathrm{l/s} \;=\; 2.92 \times 10^3\,\mathrm{cm^3\,s^{-1}}.$$

^{3}He jet target thickness III

Thickness from cell balance (triangular $\rho(z)$ about center)

- **Steady state:** particle throughput equals outflow through total conductance, hence center volume density

$$\rho_0 = \frac{I}{C_{\text{tot}}} \tag{25}$$

- **Areal density along full cell length ℓ_t:**

$$d_t = \frac{1}{2}\,\rho_0\,\ell_t = \frac{1}{2}\,\frac{I\,\ell_t}{C_{\text{tot}}}. \tag{26}$$

- **Numerical result** (77 K, ^{3}He):

$$d_t \approx 1.0 \times 10^{12}\ \text{atoms}\,\text{cm}^{-2}. \tag{27}$$

- Result scales as $d_t \propto I\,\ell_t / C_{\text{tot}}$.